Aus dem

Department für Augenheilkunde Tübingen

Universitäts-Augenklinik

The Effect of OFF-Pathways on the Human ERG Oscillatory Potentials

Inaugural-Dissertation
zur Erlangung des Doktorgrades
der Medizin

der Medizinischen Fakultät
der Eberhard Karls Universität
zu Tübingen

vorgelegt von

Passauer, Johannes Karl Andreas David

2026

Dekanin:	Professorin Dr. S. Y. Brucker
1. Berichterstatter:	Privatdozent Dr. K. Stingl
2. Berichterstatter:	Professor Dr. T. Euler
Tag der Disputation:	20.07.2026

Für

Helga und Gerhard.

Table of Contents

List of Figures and Tables

List of Abbreviations

AC:	Amacrine Cell
AMD:	Age-Related Macular Degeneration
APB:	2-Amino-4-Phosphonobutyric Acid
BC:	Bipolar Cell
BSCR:	Birdshot Chorioretinopathy
CAR:	Cancer-Associated Retinopathy
CDSRR:	Cone Dystrophy with Supernormal Rod Response
CNQX:	6-Cyano-7-Nitroquinoxaline-2,3-Dione
CRAO:	Central Retinal Artery Occlusion
CRVO:	Central Retinal Vein Occlusion
CSD:	Current Source Density
CSNB:	Congenital Stationary Night Blindness
DA:	Dark-Adapted
DA 0.01 ERG:	Dark-Adapted 0.01 $cd \cdot s \cdot m^{-2}$ ERG
DA 10 ERG:	Dark-Adapted 10 $cd \cdot s \cdot m^{-2}$ ERG
DA 3 ERG:	Dark-Adapted 3 $cd \cdot s \cdot m^{-2}$ ERG
DR:	Diabetic Retinopathy
ERG:	Electroretinography
ESCS:	Enhanced S-Cone Syndrome
ffERG:	Full-Field Electroretinogram
FIR:	Finite Impulse Response
GABA:	Gamma-Aminobutyric Acid
GC:	Ganglion Cell

GCL:	Ganglion Cell Layer
GlyT1:	Glycine Transporter Type 1
HC:	Horizontal Cell
Hz:	Hertz
INL:	Inner Nuclear Layer
IOFB:	Intraocular Foreign Body
IPL:	Inner Plexiform Layer
ISCEV	International Society for Clinical Electrophysiology of Vision
ISCEVEP:	ISCEV Extended Protocol
KA:	Kainic Acid
Kir:	Inwardly Rectifying K+ Channels
LA:	Light-Adapted
LA 30 Hz ERG:	Light-Adapted 30 Hz Flicker ERG
LA 3 ERG:	Light-Adapted 3 $cd \cdot s \cdot m^{-2}$ ERG
MAR:	Melanoma-Associated Retinopathy
mfERG:	Multifocal Electroretinogram
MG:	Müller Glia Cell
Nfia:	Nuclear Factor One a
NFL:	Nerve Fiber Layer
NMDA:	N-Methyl-D-Aspartic Acid
OCT:	Optical Coherence Tomography
ONL:	Outer Nuclear Layer
OP:	Oscillatory Potential

OPL:	Outer Plexiform Layer
PDA:	Cis-2,3-Piperidine-Dicarboxylic Acid
PERG:	Pattern Electroretinogram
PhNR:	Photopic Negative Response
PNR:	Proximal Negative Response
RBC:	Rod-Bipolar Cell
RP:	Retinitis Pigmentosa
RPE:	Retinal Pigment Epithelium
STR:	Scotopic Threshold Response
TTX:	Tetrodotoxin
VEGF:	Vascular Endothelial Growth Factor
VUS:	Variant of Uncertain Significance

1 Introduction

1.1 Basic Anatomy and Physiology of the Retina

1.1.1 Anatomy

The retina is a complex neuronal tissue which converts light into an electrical response. Simultaneously, the response is extensively processed within the retina. Many different cells contribute to this intraretinal processing. Retinal orientation is described along several axes. Relative to the path of light, regions reached first are termed proximal or inner, whereas those encountered later are distal or outer. With respect to the macula, areas are further classified as central or peripheral. Starting distally, the retinal pigment epithelium (RPE) bordering Bruch's membrane forms the first retinal layer. By regenerating the visual pigment and renewing the outer segments of the photoreceptors, it is essential for their metabolism. Mainly two types of photoreceptors can be distinguished. Whilst rods determine scotopic vision, cones are responsible for color vision in photopic conditions. In response to light, photoreceptors hyperpolarize, so that their signaling to bipolar cells (BC) changes. BCs conduct the response to ganglion cells (GC), whose axons unite to form the optic nerve. Additionally, responses are modulated by two types of lateral interneurons, the amacrine cells (AC) and horizontal cells (HC). Providing structure and metabolic conditions, Müller glia cells (MG) span the entire retina.

The retina's characteristic layering emerges from the arrangement of these cells. The outer segments, which are embedded in the pigment epithelium, and the inner segments of the photoreceptors form the photoreceptor layer. Between this layer and the outer nuclear layer (ONL) containing the photoreceptor nuclei, there is the small outer limiting membrane. Synapses between photoreceptors and BCs are located in the outer plexiform layer (OPL), in which HCs execute their feedback function. BC, HC and AC cell bodies reside in the inner nuclear layer (INL). BCs, GCs and ACs communicate in the inner plexiform layer (IPL). GCs predominate in two layers, with their nuclei forming the ganglion cell layer (GCL)

and their axons composing the nerve fiber layer (NFL). The proximal border of the retina is the internal limiting membrane, to which the endfeet of the MGs contribute. These cells and layers are illustrated in Figure 1.

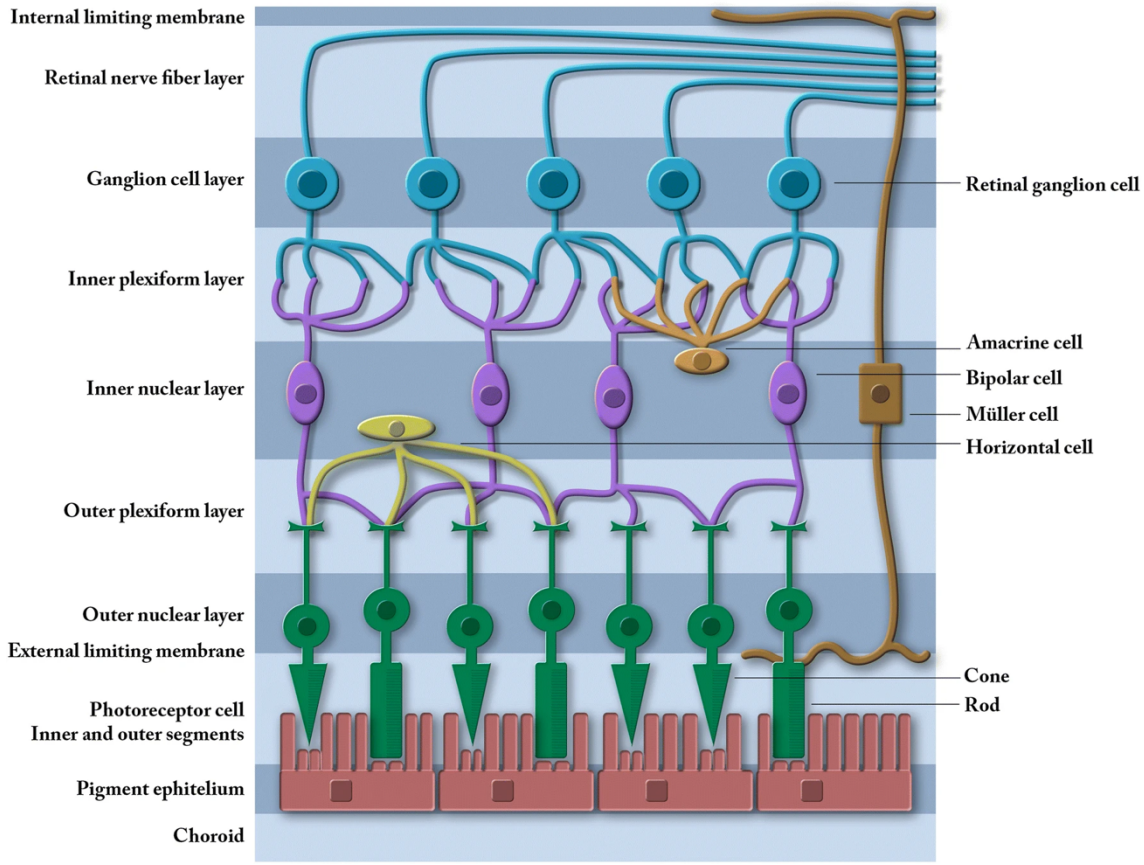

Figure 1 - Retinal Layers
Illustration of the layers and cells constituting the retina. From top to bottom, equal to the direction of the incoming light, the retinal layers are arranged as follows: the internal limiting membrane as the most proximal layer, the NFL, the GCL containing GC nuclei, the IPL, the INL containing the nuclei of ACs, HCs and BCs, the OPL, the ONL containing photoreceptor nuclei, the external limiting membrane, the photoreceptor layer and the pigment epithelium. Reproduced from Cerveró, A., Casado, A., and Riancho, J., 'Retinal changes in amyotrophic lateral sclerosis: looking at the disease through a new window', J Neurol, 268, 2083–2089, 2021, Springer Nature. Reproduced with permission from Springer Nature.

1.1.2 Physiology

As indicated in Figure 1, light traverses almost every retinal layer until it reaches the site of phototransduction, the photoreceptors. Without light, photoreceptors are depolarized and constantly emit the neurotransmitter glutamate, which results in the dark current. In return, light induces a complex process inside the photoreceptors, leading to a hyperpolarization and thus reducing the release of glutamate. Subsequent steps depend on the type of photoreceptor. Cones

synapse with two types of BCs, ON-BCs and OFF-BCs. ON-BCs express inhibitory glutamate receptors, so that the reduced liberation of glutamate following photoreceptor hyperpolarization results in a depolarization of ON-BCs. Vice versa, OFF-BCs are hyperpolarized by lesser glutamate since they express excitatory glutamate receptors. Due to this BC separation, information from photoreceptors reaches GCs via two different pathways, the ON- and OFF-pathway. Rods synapse with specific rod BCs (RBC) possessing inhibitory glutamate receptors. Those, however, do not directly synapse with GCs but rely on ACs to convey their information to GCs via cone BCs. Out of many different types of ACs, the glycinergic AII and gamma-aminobutyric acid (GABA)-ergic A17 connect the RBCs with cone BCs. Whilst the AII-AC transmits information to ON-BCs via gap junctions and OFF-BCs via chemical synapses, the A17-AC forms reciprocal synapses with RBCs as a feedback mechanism. At a brighter light intensity, another AC releases dopamine to uncouple the gap junctions between AII-ACs, consequentially reducing the influence of RBCs (Kolb 2006). This underlines the complexity of ACs and the IPL, to which an integral role in the generation of oscillatory potentials (OP) is ascribed. ACs also participate in the center and surround organization, which enables high contrast vision, through lateral inhibition. The main principle of the retina's center and surround organization is that a light stimulus in the center of an ON receptive field has an excitatory influence, whilst the stimulus has an inhibitory influence if located in the field's surrounding. The organization is ultimately represented by the GCs, which collect the whole retina's information and are divided into ON-center and OFF-center. More distally, in the OPL, the HC network contributes to the organization by giving lateral inhibitory feedback to both photoreceptors and BCs based on the information they receive from a high number of cones.

1.2 Electroretinogram

1.2.1 What is Electroretinography?

As displayed in the previous section, light stimulation evokes complex intraretinal processes involving electrical activity, which can be measured.

Electroretinography is the procedure utilized to record this electrical activity. The resulting recording of the potential caused by the electrical response is termed electroretinogram (ERG) (Armington 1988). Since the abbreviation “ERG” is often used to describe both terms, for simplicity, the same practice is adopted in this dissertation.

The retina’s reaction can be recorded as the summation of extracellular currents resulting from cell membrane conductance changes of the stimulated cells (Perlman 1995). Although all types of retinal neurons produce extracellular currents depending on the light stimulation, not all of them are equally involved in the formation of the ERG signal (Frishman 2006). To be precise, these cells must be organized in a specific order for being able to create a unidirectional flow which suffices to be measured. Regarding the ERG, due to the photoreceptors’ parallel arrangement, the relevant extracellular currents are those directed radially to the retina. Thus, as mentioned above, selected cell types such as the photoreceptors, the BCs or the MGs contribute more to ERG recordings than laterally oriented cells like ACs or HCs. These cells are the sources from which the extracellular currents find their way into the extracellular space until they leave it at a different depth in the retina, named sink. Therefore, as can be expected, a major part of the current stays within the retina. Nevertheless, the other, tinier fraction exits the retina, traversing vitreous, the sclera and the choroid until it reenters the retina through the RPE. In consequence, the extracellular currents can be divided into two separate pathways, the local path remaining in the retina, whilst the other path is the remote pathway (Perlman 1995).

Knowledge about these pathways is pivotal for understanding how the ERG measurement works. In clinical settings, the most common technique is to place the active electrode onto the cornea and the reference electrode remotely (Frishman 2006), e.g. on the forehead. This demonstrates the importance of the remote pathway, with the active electrode being placed within it, when it comes to clinical application and non-invasive studies. Moreover, any alterations to the components along the pathway will also affect the ERG’s quality, especially when the resistance along the pathway changes. This becomes evident when the vitreous humor is replaced by other substances such as silicone oil after

vitrectomy, which significantly decreases the ERG's amplitude (Foerster et al. 1985). Nevertheless, the local pathway is not merely of theoretic value either, because ERG recordings out of different retinal depths offer an important scientifical benefit (Yanagida et al. 1986). They have played a decisive role in exploring the origins of different ERG components, although there are certain limitations to be noted. Most importantly, they tend to simplify the complex structure of the retina as the measurement only captures one specific spot at a time. Additionally, a common limitation intraretinal recordings share with other methods for ERG exploration is that they are usually performed on animal material. These two previously named limitations also apply to single cell recordings, which can be used to study the origins of the ERG, as well (Frishman 2006). Furthermore, knowledge about the properties of ERG components can be obtained by pharmacological manipulation, as prominently shown by Granit (1933), whose work will be referred to in subsequent sections of this dissertation. With increasing knowledge about the variety of ion channels, neurotransmitters and microcircuitry related to retinal cells, the possibilities of pharmacological techniques to dissect the different ERG components has grown. At last, another relevant approach is to examine retinal diseases and particular lesions that affect the way the retina reacts to a stimulus, including knockout mutations as well. For instance, studying the consequences of a lack of the transcription gene nuclear factor one a (*Nfia*) revealed its importance for AII-ACs and OPs (Keeley et al. 2023).

1.2.2 Full-Field Electroretinogram

In addition to the scientific background and exploration of the ERG, the clinical perspective should be portrayed as well. For clinical application, the international society for clinical electrophysiology of vision (ISCEV) publishes standards which depict electrophysiological testing methods. These include three clinical standard tests, the full-field ERG (ffERG) (A. G. Robson et al. 2022), pattern ERG (PERG) (Thompson et al. 2024) and multifocal ERG (mfERG) (Hoffmann et al. 2021), which rely on the principle of ERG. Since it is the method underlying the

experiments described in this work, the emphasis will be laid on the ffERG. Nevertheless, other electroretinography tests will be shortly portrayed, as well.

The ffERG results from stimulating the retina with a Ganzfeld (whole-field) stimulator. As suggested by the devices name, by stimulating the entire retina, this evokes a “mass electrophysiological response” (A. G. Robson et al. 2022). The ability of the Ganzfeld stimulator to provide a homogenous distribution of a flash across the largest possible area of the retina makes the ffERG a unique test to globally measure the retina’s function (Khan 2023). The photoreceptor cells play a pivotal role for the ffERG response, so their distribution across the whole retina explains from which retinal area the response originates. Despite the fact that photoreceptor density is highest in the central retina due to the extremely high cone density, the majority of photoreceptors, mainly rods, resides peripherally (Curcio et al. 1990). Consequently, ffERG responses serve as an indicator if a disease affects generalized retinal function, whereas limited macular diseases usually do not appear with an altered ffERG response (Calcagni et al. 2024). PERG and mfERG are to be preferred for electrophysiological evaluation of macular function (A. G. Robson et al. 2018). Additionally, by differentiating between the ERG components, which will be described in a following section, ffERG allows separate assessment of outer and inner retinal function. Moreover, the ffERG provides distinction between the function of both types of photoreceptors, which is achieved by varying stimulus conditions between the six specific recordings included in the ISCEV standard (A. G. Robson et al. 2022).

The six standard ffERG recordings can be divided into two groups defined by their respective retinal adaptational state: dark-adapted (DA) and light-adapted (LA). To ensure consistent retinal adaptation between subjects, prior to the corresponding DA measurements, at least 20 minutes of dark adaptation are necessary. The following recordings are carried out with increasing stimulus strength, starting with the DA 0.01 $cd \cdot s \cdot m^{-2}$ ERG (DA 0.01 ERG). This helps to avoid interference between the stronger flashes and the DA retina. A normal response to the DA 0.01 ERG stimulus is shown in the top left corner of Figure 2, which exhibits typical exemplary responses to all six standard ffERG recordings.

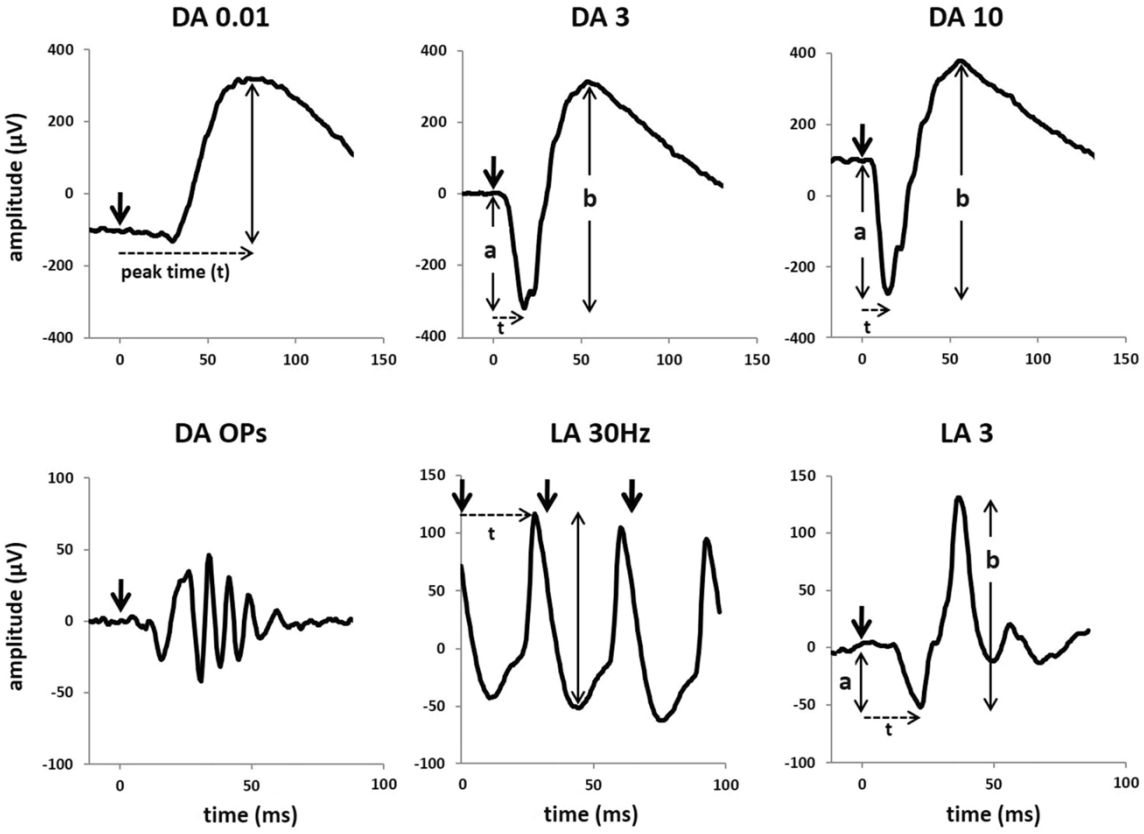

Figure 2 - ISCEV Standard ERGs

Illustration of the six standard ERGs defined by the ISCEV. Amplitudes (µV) are displayed on the y-axis, time (ms) on the x-axis. The stimulus onsets are marked by bold arrows. Horizontal broken lines indicate the convention for measuring peak times, vertical arrows for measuring amplitudes. Reproduced from Robson, A. G., et al. (2022), 'ISCEV Standard for full-field clinical electroretinography (2022 update)', Doc Ophthalmol, 144 (3), 165-77. under the Creative Commons Attribution 4.0 International License (CC BY 4.0).

As the DA 0.01 ERG flash is too dim to exceed the cone system threshold, the rod system exclusively contributes to the response (A. G. Robson et al. 2022). The other two DA stimuli, DA 3 cd·s·m^{-2} ERG (DA 3 ERG) and DA 10 cd·s·m^{-2} ERG (DA 10 ERG), stimulate both rods and cones thus resulting in a mixed rod-cone response (Frishman 2006). Nevertheless, the rod system remains the major contributor to the DA reactions in these two recordings. The DA OPs do not require an individual stimulus to be recorded because they are typically extracted from the DA 3 or DA 10 ERG measurements. If measured after DA testing, the photopic recordings will require a light adaptation of at least 10 minutes. The LA testing relies on the cone system function. It is not critical in which order the LA measurements are carried out. For the light adapted 30 Hz flicker ERG (LA 30 Hz ERG), a sequence of short 3 cd·s·m^{-2} stimuli is conducted with a frequency of

around 30 Hz, while the subject's eyes are saturated by a 30 cd·s·m^{-2} background illumination. The second photopic measurement equally uses the 30 cd·s·m^{-2} background illumination. On top of this background, a 3 cd·s·m^{-2} flash serves as stimulus for the LA 3 cd·s·m^{-2} ERG (LA 3 ERG).

1.2.3 Components of the ffERG

As indicated in the previous section, stimulus conditions decisively determine the cellular origins of the ffERG components. The main components occurring in the ffERG are those shown in Figure 2: a-wave, b-wave, the flicker responses and the OPs, which will be addresses separately. They are accompanied by minor components such as c-wave, d-wave, scotopic threshold response (STR), M-wave and proximal negative response (PNR). A groundbreaking work towards the exploration of the ERG components was delivered by Granit (1933), who demonstrated altered electrical retinal responses by deepening the anesthesia of cats. More precisely, with increasing depth of anesthesia, he reported the gradual disappearance of ERG components, naming them P-I, P-II and P-III in the order of their disappearance. Vanishing first, P-I describes a slowly rising wave. P-II is characterized by a sharp, high-amplitude first peak followed by a quick decrease which turns into a marginally rising wave before reaching the baseline. Remaining after the removal of P-I and P-II, P-III is a flat negative wave which maintains its level until the stimulus is turned off. P-III consists of a fast and a slow component (Frishman 2006). Granit's findings were fundamental for identifying the origins of the subsequently described ERG waves.

The negative deflection which typically appears first after light onset is called a-wave. It is the major component of Granit's P-III (Perlman 1995). Based on the evidence presented below, photoreceptors were identified as the source of the a-wave. Naturally, the relative contribution of the type of photoreceptor differs depending on the conditions, with cones predominating in photopic conditions and rods having a stronger influence in a scotopic environment. Brown and Wiesel (1961) used intraretinal recordings exploring the a-wave origin. Since they found the maximal a-wave amplitude in the distal retina, they attributed it to the

photoreceptors. Moreover, the rod outer segments produce a “photocurrent”, i.e. the termination of the dark current, which possesses the same shape as the a-wave (Penn and Hagins 1969). Pharmacological studies supported these findings by isolating the photoreceptors from postreceptoral cells, especially BCs, by inhibiting the signal transfer to them. These studies revolved around L-glutamate, the neurotransmitter emitted by photoreceptors: applying sodium aspartate, Sillman et al. (1969) obtained an isolated P-III response. Also, 2-amino-4-phosphonobutyric acid (APB) could selectively abolish the b-wave by blocking the transmission to ON-BCs (Massey et al. 1983). However, a study conducted by Bush and Sieving (1994) about the influence of Cis-2,3-piperidine-dicarboxylic acid (PDA) indicated the influence of cells other than the photoreceptors, i.e. postreceptoral cells, on the a-wave. PDA markedly decreased the photopic a-wave, especially in low stimulus intensities. This effect was attributed to inhibited hyperpolarizing OFF center BCs and HCs, which were consequently made responsible for a portion of the photopic a-wave in low-intensity stimuli. The cones’ contribution increases with rising intensities (J. G. Robson et al. 2003). For the DA a-wave, studies which also employed PDA and APB, suggested a modulation by postreceptoral components but demonstrated that the major generator of the scotopic a-wave are the rods (Jamison et al. 2001; Kang Derwent and Linsenmeier 2001).

In a physiological ERG response, the negative a-wave is terminated by the ascension caused by the b-wave, which is closely connected to P-II. It is considered the most important ERG component because of its role in clinical applications and the proportion it possesses in the ERG (Perlman 1995). Consequently, the scientific interest and effort towards revealing its cellular origin has been substantial, but, at the current state, not entirely conclusive. Discussing the respective contribution to the b-wave, most research points towards two types of cells: depolarizing ON-BCs and the MGs. Using a current source density (CSD) analysis, Faber (1969) was first in connecting the origin of the b-wave to the MGs. As MGs reach across all retinal layers (Fu et al. 2015), they could explain his reports of a b-wave sink in the OPL, with the source being located proximally and distally to it. Another microelectrode study by Miller and Dowling (1970),

performing intracellular MG recordings, found further evidence in favor of the MGs' involvement. It showed that the MG response did not only produce a waveform resembling the b-wave but also had a similar latency and behavior in terms of relation between stimulus and amplitude. These findings led to the development of the K^+-MG hypothesis. It proposes that the process induced by a light stimulus causes changes of K^+ concentrations. Subsequently, the MGs are depolarized by the ion changes which lead them to create a current flow which can be recorded as the b-wave. Retinal K^+ activity was intensely scrutinized considering its involvement in the b-wave generation, including the discovery of both a distal and proximal extracellular K^+ increase caused by a light stimulus (Dick and Miller 1978). Whilst the ON-BCs were supposed to cause the distal K^+ increase, ACs and GCs were assigned to the proximal increase (Dick and Miller 1985; Dick et al. 1985). Pharmacological studies lead Dick and Miller (1985) to assume that the ON-BCs create the distal K^+ increase which depolarizes the MGs. However, some controversy revolved around the origin and significance of these two extracellular K^+ increases. From detecting that applying APB abolished both K^+ increases, Stockton and Slaughter (1989) concluded both originated from the ON-BCs. Microelectrode recordings from Karowski and Proenza (1977), who scrutinized MG responses in relation to K^+ changes and transretinal potentials, suggested a proximal MG depolarization and argued against MGs causing the b-wave. Using a computer model simulating the retina, Newman and Odette (1984) claimed that although the proximal K^+ increase was larger than the distal increase, the latter was decisive for the b-wave, thus supporting the K^+-MG hypothesis. Moreover, the application of Ba^{2+}, a blocker of the inwardly rectifying K+ (Kir) channels, resulted in a partial reduction of the b-wave (Wen and Oakley 1990). Given the importance of the Kir channels for MGs (Newman 1993), this served as further evidence for their contribution. A similar effect of Ba^{2+} was observed in a study by Xu and Karwoski (1994). However, by combining it with CSD analyses, they revealed that Ba^{2+} only blocks the proximal source attributed to other ERG components, M-wave and slow P-III, caused by MGs, without affecting the distal sink associated with the b-wave. These results were in accordance with the fact that APB, as opposed to Ba^{2+}, totally eliminated the b-

wave, indicating a close connection to the ON-BCs (Gurevich and Slaughter 1993). Further evidence advocating in favor of the ON-BCs' relevance for the b-wave was obtained by isolating P-II, which as mentioned earlier, reflects the b-wave. J. G. Robson and Frishman (1998) acquired isolated P-II by removing the contribution of more responsive proximal retinal cells using N-Methyl-D-aspartic acid (NMDA) and subtracting the photoreceptor component, which had previously been isolated with APB and 6-cyano-7-nitroquinoxaline-2,3-dione (CNQX). Isolated P-II was divided into a leading fast and a slow, Ba^{2+}-sensitive component. Whereas the latter was attributed to the MGs, fast P-II reflects the ON-BC response. To date, the ON-BCs are considered the major drivers of the b-wave (Dmitriev et al. 2021). That is also reflected in the current ISCEV standard, which solely names the ON-BCs as b-wave origin (A. G. Robson et al. 2022). Nevertheless, the MGs remain a possible modulator of the b-wave, especially because of the various observations on the Kir channels (Bhatt et al. 2023).

Besides the ERG responses evoked by the onset of a light stimulus, there is also an ERG component induced by the stimulus offset (Frishman 2006). This positive deflection is termed d-wave. It is typically recorded under photopic conditions. Though, using mesopic stimuli also enables eliciting a small d-wave under DA conditions which most likely results from interaction with the cone pathway (Naarendorp and Williams 1999). The application of long-duration flashes may be necessary to separate the d-wave from other components (Frishman 2006). Regarding the origin of the d-wave, an influence of different retinal components was shown. Amongst them, the most important element is the cone OFF-pathway, especially for the d-wave's fast initial part, given the effect of PDA application (Ueno et al. 2006). This is in accordance with the findings of Sieving et al. (1994) and CSD analyses, which also revealed the importance of the OFF-BCs (Xu and Karwoski 1995). Contributions to the d-wave were also attributed to cone photoreceptors due to microelectrode (Yanagida et al. 1986) and CSD (Xu and Karwoski 1995) studies. After combined application of PDA and APB, cones were identified as pivotal for the late phase of the d-wave (Ueno et al. 2006). Opposing the OFF-pathway's effect, the cone ON-pathway modulates the d-wave

(Ueno et al. 2006). Lastly, inner retinal components to a smaller amount modify the d-wave, inferring from studies with tetrodotoxin (TTX) and NMDA modulation (Awatramani et al. 2001; Ueno et al. 2006).

Because of their little importance in the context of this thesis, further ffERG components will only be addressed briefly. As part of the standard ISCEV ffERG protocol, the LA 30 Hz ERG mainly reflects the activity of cone ON- and OFF-BCs but also requires the long- and medium-wavelength sensitive cones (A. G. Robson et al. 2022).

The c-wave consists of two subcomponents, a cornea-positive corresponding to Granit's P-I, which is elicited by the RPE (Perlman 1995) and a cornea-negative component corresponding to the slow part of P-III, which reflects MG activity. As the first component is mostly larger, the c-wave characteristically is a slow cornea-positive wave following the b-wave (Frishman 2006).

Under particular recording conditions, even more components like the STR, the M-wave and the PNR may be recorded in scientific contexts (Perlman 1995).

1.2.4 Clinical Use of the ffERG

Despite the growing significance of other diagnostic modalities in ophthalmology, such as optical coherence tomography (OCT), the ffERG continues to occupy an essential role owing to its importance in clinically assessing global retinal function (Khan 2023). In the overall perspective, as indicated afore, the ffERG facilitates the assessment whether retinal conditions are rod- or cone-specific along with determining if a condition affects the entirety of the retina or solely the macula. A variety of conditions which influence the retina are accompanied by ffERG alterations with some strongly relying on the ffERG as a diagnostic pillar. However, only few of them show pathognomonic ffERG alterations (Vincent et al. 2013). The list of pathognomonic ERGs comprises the enhanced S-cone syndrome (ESCS) which was first described by Marmor et al. (1990). It is characterized by the absence of a response in the DA 0.01 ERG, reduced LA 30 Hz ERG amplitudes (Vincent et al. 2013) and markedly prolonged implicit times

(Marmor et al. 1990). One of the most characteristic features is the close resemblance between scotopic and photopic ERG responses (Marmor et al. 1990). Another disorder with pathognomonic ffERG findings is the cone dystrophy with supernormal rod response (CDSRR) or *KCNV2* retinopathy, first described by Gouras et al. (1983). A defining property of CDSRR is the broadened waveform of the a-wave followed by a relatively high-amplitude b-wave in the mixed rod-cone responses. Responses to low-intensity stimuli are typically diminished. Characteristically, b-wave amplitudes show a supra-linear increase to increasing the luminance (Michaelides et al. 2005). Photopic ERGs are typically delayed and decreased (Vincent et al. 2013). Furthermore, a disorder called “bradyopsia” also offers pathognomonic ERG abnormalities. It was first described by Kooijman et al. (1991), who observed an extended duration of the suppression a second stimulus receives following the first stimulus. However, since the ISCEV standard ffERGs may even be misleading, detecting its pathognomonic findings requires measurements extending beyond the standard protocols (Vincent et al. 2013).

Apart from these three exceptional examples, ffERG is frequently applied in the assessment of hereditary disorders. With modern multigene panel screenings, functional assessments such as ffERG guide the focus of the genetic testing and may explain variants of uncertain significance (VUS) (Cornish et al. 2021). A prominent example is retinitis pigmentosa (RP) which mostly originates from a hereditary cause. As syndromic form, it may also occur as part of syndromes, so that the ffERG delivers important information about retinal function in various affected diseases (Yu et al. 2025). Typical ffERG findings are markedly reduced amplitudes in all standard recordings with delayed b-wave implicit times, which deteriorate or even become nonrecordable with disease progression (Huang et al. 2023). Sabbaghi et al. (2021) additionally demonstrated a criterion based on the time-frequency analysis of ffERG recordings to better distinguish between normal and RP responses even in the early stage. Congenital stationary night blindness (CSNB) serves as another example of an inherited disorder in which ffERG is diagnostically essential (Durajczyk and Lubinski 2025). The ffERG enables differentiation between the types of CSNB (Zeitz et al. 2018). The

missing a-wave in the mixed rod-cone ERGs separates Riggs type from Schubert-Bornschein type, in which the normal a-wave combined with a notably reduced b-wave result in an electronegative pattern (Tsang and Sharma 2018). Schubert-Bornschein, the more prevalent type, is further subdivided into a complete and incomplete subtype. On the one hand, complete CSNB, presents with nonrecordable rod ERG responses and OPs alongside nearly normal cone ERG responses. On the other hand, reduced but detectable rod ERG responses, recordable OPs but markedly diminished cone responses characterize the incomplete type. Both present with electronegative mixed rod-cone responses (Miyake 2006).

The evaluation and management of inflammatory ocular disorders also relies on the use of electrophysiological methods such as the ffERG (Yu and Kurup 2024). Among uveitic disorders, Birdshot chorioretinopathy (BSCR) possesses a unique waveform as its disproportionately reduced b-wave results in a low b/a ratio (Hirose et al. 1991). The LA 30 Hz ERG implicit time is essential in BSCR both as a consistent diagnostic parameter and to monitor the course of the disease (Comander et al. 2011). BSCR is part of the white dot syndromes, a group of disorders characterized by inflammation of RPE and choroid (Pohlmann et al. 2019), for which ffERG provides valuable insight into retinal function (Yu and Kurup 2024). Additional autoimmune retinopathies include the paraneoplastic melanoma-associated (MAR) and cancer associated retinopathies (CAR) (Hall and Volpe 2008). Since different cancers may be accompanied by CAR, it offers diverse ffERG findings and electrophysiological evaluation can be prognostically relevant (Neveu et al. 2025). Beside other ffERG features, MAR exhibits the electronegative waveform known from CSNB (Keltner et al. 2001). Because of the functional retinal alterations in multisystemic inflammatory disorders like Vogt–Koyanagi–Harada disease (Sakata et al. 2019) and Behçet's disease (Cruz et al. 1990), the ffERG possesses selective applications in these diseases, as well. Though, one should not disregard that the ffERG rather belongs to extended diagnostics than to routine testing in ocular inflammatory disorders (Moschos et al. 2014).

In retinal vascular occlusion, i.e. central retinal vein occlusion (CRVO) or central retinal artery occlusion (CRAO), ffERG responses can be of prognostic relevance. Whilst reduced OP amplitudes are an early indicator for CRVO (Qu et al. 2024), reduced b/a ratio (Williamson et al. 1997) and b-wave amplitude (Hayreh et al. 1989) predict ischemic CRVO, which deteriorates the prognosis. In CRAO, multiple ERG parameters can serve as predictors of a better visual outcome. These include the DA 3 ERG b-wave amplitude, b/a ratio and photopic negative response (PhNR) amplitude, especially if they are combined (Kim et al. 2020a), and a normal to supernormal LA 30 Hz ERG amplitude (Kim et al. 2020b).

The ffERG can be a useful instrument to estimate toxic retinal damage, for instance in ocular siderosis caused by an intraocular foreign body (IOFB) (O'Neill and Smith 2021). All standard ffERG recordings are reported to show subnormal amplitudes with b-wave (Knave 1969) and OPs (Hope-Ross et al. 1993) being particularly affected. FfERG parameters are not merely useful to predict visual outcome by analyzing the OP amplitudes prior to surgery (Mai et al. 2021), but also enable monitoring: decreasing amplitudes without removal of the IOFB (Schechner et al. 1990) or possible improvement due to surgery (Imaizumi et al. 2000; Kannan et al. 2016). FfERG may also reveal functional retinal impairment caused by alcoholic substances in the form of methanol poisoning (McKellar et al. 1997), alcohol addiction (Xie et al. 2022) and fetal alcohol syndrome (Hug et al. 2000). Drug toxicity represents another source of retinal damage for which the ffERG can reveal useful information. Alongside ffERG alterations in various drugs (Chiang et al. 2022; O'Neill and Smith 2021), examples can be found in the group of anticonvulsants. FfERG helps to monitor retinal function in patients treated with vigabatrin (Sergott and Westall 2011) and to assess ocular side effects in topiramate treatment (Chiang et al. 2022).

In Germany, the three leading causes of blindness are age-related macular degeneration (AMD), glaucoma and diabetic retinopathy (DR) (Finger et al. 2011). Despite not being part of the standard diagnostics, electroretinographic testing can play a role in these common diseases. In AMD, ffERG alterations suggest that retinal impairment exceeds the macula (Forshaw et al. 2022). Following anti-vascular endothelial growth factor (VEGF) injection, ffERG showed

improved responses (Skaat et al. 2011), so that it could be useful monitoring the response to anti-VEGF treatment (Galuszka et al. 2023). However, mfERG delivers more detailed spatial information in AMD (Neveu et al. 2025). Whereas standard ffERG recordings are of minor relevance in glaucoma, the PhNR (Preiser et al. 2013) and PERG may enable early detection of glaucomatous damage (Meigen and Bach 2006). Regarding the neural degeneration in DR which can be measured with ffERG, there is a considerable number of clinical studies (McAnany et al. 2022). In a recent study, the OPs, particularly the implicit time of OP_2, were found to sensitively distinguish different stages of DR and show alterations in diabetics even before vasculopathy (Ba-Ali et al. 2022). Furthermore, LA flicker ERG has become increasingly interesting for the management of early DR, not least because of the implementation of a portable ERG instrument (McAnany et al. 2022). This device, which apparently is as reliable as conventional ffERG in different diseases (Carter et al. 2021), could increase the accessibility of ffERG (Neveu et al. 2025) and also be beneficial for health care systems (Bayer et al. 2025).

It should be noted that although ffERG possesses numerous applications, it is rarely exclusively used in the diagnostic process and should be interpreted together with other diagnostic methods to obtain a reliable diagnosis (Yap et al. 2015). These include, alongside non-electrophysiological diagnostics, other ERG methods, such as those depicted in the following section.

1.2.5 Alternative Electroretinography Methods

One of these additional electroretinographic tools is the PERG, for which a high contrast checkerboard with rapidly reversing black and white fields serves as stimulus. Depending on the temporal frequency of the contrast reversals, a steady-state or transient response can be acquired. The latter is obtained in the ISCEV standard PERG (Thompson et al. 2024). Unlike in the ffERG, the PERG predominantly represents a response from the macula, thus being a sensitive tool in macular dysfunction (Holder 2006). For clinical use, two characteristic components, P50 and N95, constitute the PERG response. Their nomenclature

derives from respective polarities and peak times (Bach and Hoffmann 2006). P95 permits a precise evaluation of GC function. While N50 is predominantly elicited by the GCs, it is also influenced by more distal retinal elements. Given that PERG, despite the pivotal role of the GCs, is dependent on cone function, P50 provides insights into the functional status of the macular cones (Thompson et al, 2024). Moreover, a chronic GC damage could present with a reduced peak time and amplitude of P50. In combination with ffERG, PERG enables differentiation between a generalized retinopathy and one confined to the macula. Furthermore, PERG can serve to rule out macular dysfunction as the underlying cause of pathological visual evoked potentials (A. G. Robson et al. 2018).

MfERG represents the third major electrophysiologic technique for retinal evaluation. Unlike ffERG and PERG, with mfERG, a topographic representation of retinal function may be obtained (Hoffmann et al. 2021). It provides a map of multiple ERG responses to enable assessment of the localization of retinal dysfunction. To receive these responses, typically 61 or 103 hexagons are arranged side by side with their switching between light and dark serving as stimulus. The predetermined, “pseudorandom” order in which each hexagon’s status alternates is called m-sequence. All hexagons have the same m-sequence but start at a different point so that their timing is shifted relative to each other (Hoffmann et al. 2021). In fact, mfERG does not directly record an ERG from each targeted retinal area but merely a continuous ERG signal, from which the local ERG responses are derived. The underlying extraction process is a cross-correlation between the stimulation sequence and the continuous ERG signal resulting in local mfERGs, which represent the first-order kernel of the cross-correlation (Hood 2000). Due to the different stimulus conditions and the extraction process, mfERG produces a distinct waveform comprising two negative deflections, N1 and N2, between which a positive peak, P1, is interposed. However, if the temporal density of flashes is reduced, the waveform will increasingly resemble the ffERG waveform with N1 corresponding to the a-wave, P1 to b-wave and OPs (Hood 2000). Regarding the retinal origin, mfERG mostly represents the outer retina, receiving strong contributions from OFF- and ON-BCs but only small contributions from the cone photoreceptors and the inner

retina (Hood et al. 2002). MfERG is a powerful component of electrophysiologic retinal assessment, especially to localize the site of retinal dysfunction, to identify outer retinal diseases, in maculopathies (Hoffmann et al. 2021) and serves as an objective screening tool for hydroxychloroquine retinopathy (Marmor et al. 2016).

Apart from the three presented standard ERG procedures, the ISCEV also approves extended ERG protocols to target specific issues. The methods available at the time of writing are presented in the following. To scrutinize rod and rod-mediated functions in detail, the ISCEV extended protocol (ISCEVEP) for derivation and analysis of the strong flash rod-isolated ERG a-wave (Brigell et al. 2020) as well as the ISCEVEP for the stimulus–response series for the DA full-field ERG b-wave (Johnson et al. 2019) may be useful. The ISCEVEP for the S-cone ERG assesses S-cone pathways, which is helpful for diagnosis of ESCS, distinction between rod and S-cone monochromacy and other S-cone-affecting disorders (Perlman et al. 2020). Another ISCEVEP aims to evoke the maximal PhNR to evaluate GC function, which, as previously indicated, is particularly affected by glaucoma (Frishman et al. 2018). The ISCEVEP for the DA red flash ERG allows for a more thorough insight into DA cone and rod function, being diagnostically important in achromatopsia and, combined with attenuated standard LA ERGs, pathognomonic for “bradyopsia” (Thompson et al. 2018). In the ISCEVEP for the stimulus-response series for LA full-field ERG, a series of flashes with increasing intensity improves the evaluation of generalized cone function and cone-related ON- and OFF-responses (McCulloch et al. 2019). The latter likewise characterize the ISCEVEP for the photopic ON-OFF ERG which provides additional information in a variety of disorders with dysfunctional ON- and OFF-pathways (Sustar et al. 2018).

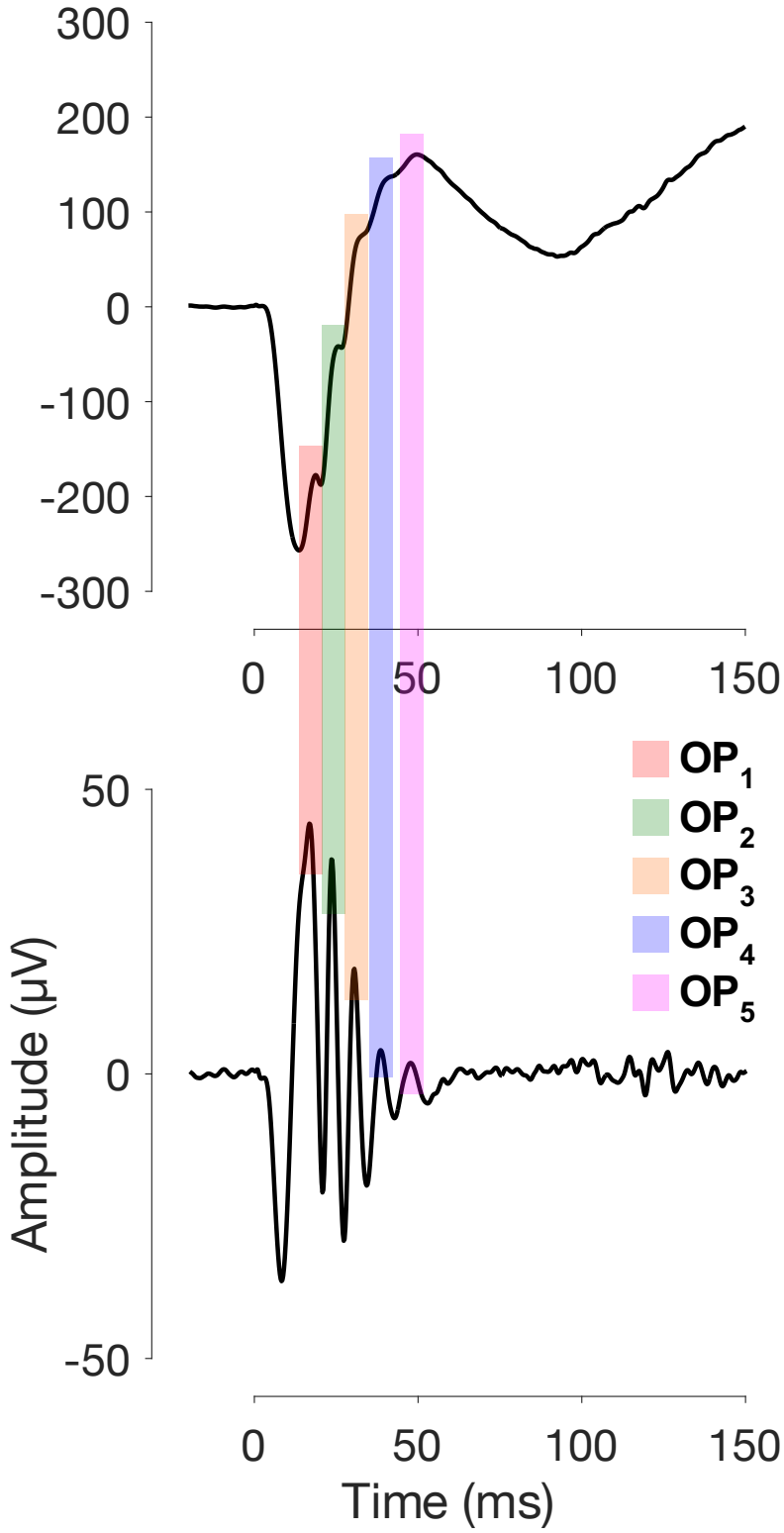

Figure 3 - Relation between OPs and B-Wave
Illustration of an ERG response above and the corresponding OPs below after application of a 75 Hz to ≥ 300 Hz band pass filter. The graph shows the amplitude (µV) on the y-axis and the time (ms) on the x-axis. Indentations on the rising limb of the b-wave are connected to their corresponding OP wavelets via bands of different colors. The first wavelet (OP_1) is indicated by the red, the second (OP_2) by the green, the third (OP_3) by the orange, the fourth (OP_4) by the blue and the fifth (OP_5) by the pink band.

1.3 Oscillatory Potentials

1.3.1 General Knowledge about the Oscillatory Potentials

The first description of a polyphasic b-wave, which technically results from the OPs, was delivered by Granit and Munsterhjelm (1937), whilst they were first identified to be a separate ERG component in humans by Cobb and Morton (1953). As illustrated in Figure 3, they are superimposed wavelets on the rising limb of the b-wave and characterized by a high frequency and low amplitude. This explains the necessity of using a band pass filter to optimally visualize them. Following the recommendations of the ISCEV standard (A. G. Robson et al. 2022), this band pass filter ranging from 75 Hz to ≥ 300 Hz should be applied to the DA 3 or DA 10 ERG measurements to obtain the OPs. However, with both rod and cone system contributing to the OPs (Peachey et al. 1987), they may also be recorded in photopic conditions. The best OP responses are obtained in mesopic conditions, when a mixed rod-cone response is elicited (Wachtmeister 1998), like in the protocols proposed by the ISCEV. The ISCEV standard also recommends excluding the first flash from being utilized for the OPs (A. G. Robson et al. 2022) because this enables the conditioning flash effect to induce a mixed rod-cone response (Wachtmeister 1998).

1.3.2 Origins of the Oscillatory Potentials

Contrary to most other ERG components, the research on the exact mechanisms responsible for the OPs has not been entirely conclusive to this point. This cannot be attributed to a paucity of research but rather the complexity of the OPs. Presumably, multiple cells are involved in their generation and account for their complexity. Nevertheless, to provide a better overview, current knowledge on the OPs will be portrayed separately for each cell of interest. Beginning with the cells who initiate the processing of the light signal, the photoreceptors offer some controversy as for their involvement in the OPs. Wachtmeister (1998) excluded their involvement because intraretinal depth studies on birds (Ogden and Wylie 1971) and monkeys (Ogden 1973) found the OPs are very prominent in the IPL and thus too proximal for the photoreceptors. Further, as opposed to

photoreceptors, who are supplied by the RPE, the OPs require retinal circulation (Brown 1968) and were shown to be reduced after blocking synaptic transmission between photoreceptors and second order neurons (Morita 1971; Wachtmeister and Dowling 1978; Wachtmeister 1981a). Contrarily, Dong et al. (2004) reported that the photoreceptors contribute directly to the first OP peaks because they were not affected by the application of APB combined with CNQX to isolate the photoreceptor response. This was later supported by Dai et al. (2017). Besides a direct photoreceptor contribution, OPs rely on the function of both types of photoreceptors. Studies on retinopathies with selective involvement of rod or cone, respectively, showed that early OPs depended more on rod function, late OPs rather on cone function (Righetti et al. 2021; Wachtmeister 1998). This suits the conclusions from (Lei et al. 2006), who explored the frequency characteristics of mice OPs. They found that the peak frequencies of rod-driven OPs and earlier OP components were higher than those of cone-driven OPs and later components. The observation that mixed rod–cone responses yield the most consistent OPs (Wachtmeister 1998) further supports the importance of both photoreceptor types.

The horizontal cells probably are excluded as OP generators because their frequency characteristics do not match the OPs (Foerster et al. 1977) and like the photoreceptors, their location does not suit to the OPs (Wachtmeister 1998). This is in accordance with pharmacological findings suggesting the horizontal cells have no more than small influence on OPs (Dong et al. 2004).

For MGs, sources agree on them not being involved in the generation of the OPs (Wachtmeister 1998). This consensus is based on intracellular MG recordings (Miller and Dowling 1970), which did not match OP responses as well as the incapacity of MGs to create extracellular currents reaching frequencies as high as those of the OPs (Ogden 1973).

Since the GCs take part in the signaling of the IPL, they should be considered when exploring the OPs. Due to their observations on optic nerve stimulation, Doty and Kimura (1963) argued against an involvement of the GCs. Additional evidence was obtained by studying diseases related to GC pathology. On the one

hand, in optic atrophy (Wachtmeister and el Azazi 1985) and glaucoma (Frishman et al. 1996; Wanger and Persson 1983), which both are associated with GC loss, no significant differences to controls could be shown. On the other, there are many examples of GC-affecting diseases in which the OPs appear altered. Earlier studies, also on glaucoma (Gur et al. 1987) and optic atrophy (Vaegan et al. 1995), revealed reduced OP amplitudes. Later, Zhou et al. (2007) conducted measurements on both glaucomatous and pharmacologically altered eyes in which retinas influenced by TTX produced, similarly to glaucomatous retinas, selectively eliminated high-frequency OPs. Recently, Barboni et al. (2024) demonstrated that both DA and LA OPs were reduced in Leber hereditary optic neuropathy, with the effect being more pronounced when filtering out lower frequencies. Further findings in favor of an involvement of the GCs comprise the co-occurrence of damaged GC dendrites and reduced OPs following the application of kainic acid (KA) (Vaegan and Millar 1994) and that OPs are associated with GC discharge (Steinberg 1966). Moreover, Haq et al. (2023) demonstrated that the activity of the GCs temporally correlated with the OPs.

The BCs are amongst the cell types most frequently associated with the OPs. An indicator of BC involvement may be inferred from the previously noted association of OPs with both types of photoreceptors, since their dichotomy is represented by BCs, as well. Moreover, BCs also initiate the division into ON- and OFF-pathways. For the OPs, a similar division tying early OP peaks to ON and later peaks to OFF components was proposed by different authors (Kojima and Zrenner 1978; Wachtmeister 1980, 1981b). Kojima and Zrenner specifically linked the last OP peak to the OFF component because it correlated with the stimulus duration and termination. Wachtmeister derived his assumption from pharmacological trials using glycine (1980) and ethanol (1981b). Since both substances had previously been shown to manipulate the OFF-pathway, their selective influence on later OPs was ascribed to the OFF-pathway (Wachtmeister 1998). In another pharmacological experiment, the application of APB to inhibit the transmission between photoreceptors and ON-BCs strongly reduced especially intermediate OPs (Guite and Lachapelle 1990). However, Dong et al. (2004) relativized the influence of the ON-BCs arguing that APB attenuated the

entire ON pathway. They revealed only a minor contribution of ON-BCs by subtracting the photoreceptor component, obtained under combined APB and CNQX application, from the response recorded with APB alone. Additional findings of their study indicated that the contribution of the OFF-pathway was very small. Recently, specifically the RBCs have received more attention. The inhibitory input to these cells via glycinergic and GABAergic transmission could be important for the OPs (Dai et al. 2017). The role of RBCs is underlined by the reduction of OPs in *Tmem30a* knockout mice, with the *Tmem30a* deficiency simultaneously leading to severely impaired RBCs (Yang et al. 2019). Employing different substances, Liao et al. (2023) found more evidence for the role of the RBCs with emphasis on reciprocal synapses they share with two types of ACs. They also mentioned that due to the findings of a study on achromatopsia (Righetti et al. 2021), OFF cone BCs could affect the OPs.

When discussing the OPs' drivers, the ACs have occupied a central role for many years so that a great amount of evidence related to them has accumulated. Intraretinal depth recordings in mudpuppies identified the first OP peak within the region between the IPL and INL, which coincides with the site where ACs operate (Wachtmeister and Dowling 1978). Numerous neurotransmitters are associated with the ACs, including dopamine, substance P, somatostatin and especially GABA and glycine (Kolb 2006). Therefore, OP alterations caused by pharmacological modulation of these transmitters was referred to the ACs. Reducing dopaminergic transmission, haloperidol attenuated mostly early OPs (Wachtmeister 1981a) whilst for reserpine, a reduction of OPs (Gutierrez and Spiguel 1973) as well as their recovery through L-Dopa (Hempel 1972) was demonstrated. Modulation of the OPs by using peptides could also be explained by participation of the ACs since somatostatin increases OP amplitudes, whilst substance P selectively decreases early OPs (Wachtmeister 1983). Moreover, OP modification by influencing the renin-angiotensin-aldosterone system was interpreted to originate from the ACs (Jacobi et al. 1994). The two predominant neurotransmitters for the ACs are GABA for the A17-AC and glycine for the AII-AC (Kolb 2006). Notably, OPs appear to be relatively sensitive to changes of those substances. Whereas the direct application of glycine resulted in reduced

OPs (Korol et al. 1975), inhibiting glycinergic transmission via strychnine had a particularly reducing effect on the later OPs (Dai et al. 2017; Wachtmeister 1980). Correspondingly, selective inhibition of glycine transporter type 1 (GlyT1) decreased the OPs likewise (Liu et al. 2014). Conflicting results have been published concerning GABA inhibition as on the one hand, attenuation of early OPs via bicuculline and picrotoxin (Wachtmeister 1980), on the other, removal of later OP components by SR95531 ($GABA_A$ antagonist) and GABA opposed to later OP enhancement by methylphosphinic acid ($GABA_C$ antagonist) (Dai et al. 2017) were reported. Nevertheless, the variable effects of diverse agents influencing different GABA subtypes on OPs (Dai et al. 2017; Moller and Eysteinsson 2003) could support AC involvement. Besides, non-pharmacological studies provide additional evidence. Midena et al. (2021) related the OP alterations found in early-stage DR to functional impairment of ACs. Keeley et al. (2023) observed that the AII-AC depletion in *Nfia* knockout mice was associated with substantially diminished OPs. Another recent study using a μERG technique pointed out the essential role of the gap junctions which interconnect ACs since carbenoxolone, a gap junction inhibitor, abolished the OPs (Haq et al. 2023).

Considering the evidence for the previously discussed distinct cell types, it is likely that the OPs do not originate solely from one cell. In fact, there is evidence for the contribution of multiple components which will be presented in this last section. An early study in favor of this theory scrutinized the intraretinal distribution of individual OP peaks, discovering that earlier peaks were localized more proximally than later peaks (Wachtmeister and Dowling 1978). This was attributed to a previously suggested feedback system within the retina (Brown 1968). A commonly found pattern within literature is separating OPs into two parts, early and late. As was alluded to before, early OPs may derive directly from photoreceptors, while both types of photoreceptors are differentially involved in earlier and later phases of the OPs. Pharmacologically, KA (Vaegan and Millar 1994), GABA blockers bicuculline and picrotoxin (Wachtmeister 1980), beta-alanine (Wachtmeister 1981b), Haloperidol (Wachtmeister 1981a), substance P (Wachtmeister 1983) have a pronounced effect on earlier OPs. Moreover, later OPs were particularly sensitive to alterations of the inhibitory transmitters glycine

and GABA, suggesting that the previously mentioned feedback system may be an inhibitory feedback system. Reciprocal synaptic connections between AII- / A17-ACs and RBCs could be the correlate to this inhibitory feedback (Dai et al. 2017; Liao et al. 2023), as implied in earlier passages. As explained before, the OFF-pathway was associated to later OPs due to their behavior when exposed to longer stimulus durations (Kojima and Zrenner 1978) and ethanol (Wachtmeister 1981b). Apart from the early-late dichotomy, many other cases illustrate OPs may present non-uniformly. Dong et al. (2004) found a distribution into early (photoreceptor-generated) intermediate (action-potential independent, slightly sensitive to TTX) and late (action-potential dependent, very sensitive to TTX) OPs. The intermediate OP_3 and OP_4 are both attenuated in CSNB and susceptible to slow flickering stimuli as reported by Lachapelle et al. (1983). By varying the recording axis by utilizing different electrode positions and visual angles, individual alterations of OPs were observed (Tremblay and Lam 1993). Rousseau and Lachapelle (1999) argued against the above-described assignment of early and late OPs to rods and cones, respectively, but proposed each OP originated from a distinct source because this could best explain their results from varying stimulus conditions. It was also shown that OPs spread into two frequency bands (Lei et al. 2006) which receive different input from inhibitory receptors (Dai et al. 2017). Recapitulating all cells and mechanisms attributed to the generation of the OPs and given the complex interconnection within the IPL, the accumulated evidence to date suggests that OPs reflect the activity of a multifactorial system.

1.4 Depiction of the Main Question

In recent years, studies on the OPs have focused particularly on the implications of pharmacological manipulation of OP responses. Simultaneously, the evidence underlining the involvement of the ACs has grown, whilst other components including the OFF-pathway have received less attention. Though, a recent study comparing healthy OP responses with those of achromats debated the involvement of OFF-cone BCs as explanation for the appearance of, albeit small,

OPs in achromatopsia (Righetti et al. 2021). However, the evidence on the involvement of the OFF-pathway in OP generation is rather small and some time has passed since the publication of the most pivotal source by Kojima and Zrenner (1978), which presumed the involvement of the OFF-pathway due to the influence of varying stimulus duration on OPs.

The present dissertation sought to investigate the question of the extent to which the OFF-pathway contributes to the generation of OPs. For this purpose, a protocol, based on the ISCEV standards for mixed rod-cone responses was implemented. In this protocol, progressively increasing stimulus durations were employed under the hypothesis that this would reveal OFF-pathway effects (Righetti et al. 2025). We implemented a time-frequency analysis using a convolution of a complex Morlet wavelet to extract the power over time and frequency for better visualization of the processes following the stimuli.

2 Material and Methods

2.1 Subjects

For the measurements, 15 healthy voluntary human participants consisting of 10 females and 5 males (median age: 27 ± 13.27) served as subjects (Righetti et al. 2025). The inclusion criteria, which had to be fulfilled to participate in the study, comprised a best corrected visual acuity of 20/20 and no ocular pathology. All participants signed a written consent and were performed with the understanding of the participants. The study was conducted in accordance with the principles of the Declaration of Helsinki and approved by the Ethics Board of the University of Tübingen under the number 284/2012BO2.

2.2 Setup and Preparation

To ensure equal conditions, all participants underwent the same preparations. After being instructed about the procedure, eye drops were applied to both eyes. The eye drops were used to provide dilated pupils (phenylephrine hydrochloride (2.5%), Mydriaticum Stulln, Pharma Stulln, Stulln, Germany) and local anesthesia of the cornea (topical tropicamide (0.5%)). Before placing the gold cup skin electrodes, the areas on which the electrodes were placed had been cleansed with an abrasive gel to remove sebum. The positions for the skin electrodes were the temples on both sides, which served as reference electrodes for the negative input of the ipsilateral eye, and the glabella, which served as the ground electrode. A conductive paste was applied between the skin and the electrodes for the purpose of reducing the impedance by improving the electrical connection. To record the positive input, silver corneal fiber electrodes (DTL-electrode, Diagnosys Ltd., Dublin, Ireland) were employed as positive electrodes and placed across the cornea along the lower lid. The impedances of the skin electrodes were scrutinized subsequent to the placement of all electrodes and skin cleansing was repeated until all electrodes showed an impedance of 5 kΩ or smaller. After finishing the preparations, all participants underwent 20 minutes of dark adaptation to create scotopic recording conditions. A ColorDome stimulator was the device used for the ffERG recordings combined with the Espion E2 software

(Diagnosys Ltd., Cambridge, UK). All participants were instructed to fixate a central red fixation spot and to not blink or move during the measurements to provide optimal recording conditions. Adherence to these instructions was ensured by monitoring the participants with an infrared camera provided with the stimulator.

2.3 Protocol

Step	Luminance (cd·s·m^{-2})	Duration (ms)
1	0.3	2
2		4
3		8
4		16
5		32
6		64
7	3	2
8		4
9		8
10		16
11		32
12		64
13	10	2
14		4
15		8
16		16
17		32
18		64

Table 1 - Study Protocol
Depiction of the protocol employed in the study. The steps are arranged in the order they were applied from top to bottom in the left column. The luminance (cd·s·m^{-2}) for the corresponding steps is displayed in the middle column. The stimulus durations (ms) are listed in the right column.

The protocol, with which all participants were stimulated, consisted of 18 steps, visualized in Table 1. These steps and their respective light stimuli shared a few basic conditions. The light stimuli consisted of a white-6500 K color temperature single pulse at a frequency of 1 Hz executed with a background illumination of 0 $cd \cdot m^{-2}$. A sampling frequency of 4000 Hz was used.

Each step was made up of 5 identical light stimuli. The main principle of increasing stimulus duration and luminance during the course of the protocol attempted to avoid falsification due to light adaptational effects. The table shows that three different flash strengths were employed. Whilst the lowest luminance, 0.3 $cd \cdot s \cdot m^{-2}$, is not part of the ISCEV standard (A. G. Robson et al. 2022), both 3 and 10 $cd \cdot s \cdot m^{-2}$ are included in the ISCEV standard, which also recommends them for recording DA OPs. Each of the three flash strengths were combined with six stimulus durations in the following order: 2, 4, 8, 16, 32 and 64 ms (Righetti et al. 2025). These stimulus durations intentionally were not chosen in accordance with the ISCEV standards, which suggest that the stimulus duration should not surpass 5 ms, to examine the effects of altering stimulus durations (A. G. Robson et al. 2022).

2.4 Data Analyses

After recording, ffERG traces from all the steps were extracted using a custom script developed in MATLAB R2023b (The MathWorks, Natick, MA, USA). For each trace, the amplitude and the implicit time of a- and b-waves were extracted. The a-wave amplitude is considered as the most negative trough following the stimulus onset, and its implicit time as the time interval from flash onset to its trough. The b-wave amplitude is identified as the most positive peak following a-wave, with its implicit time calculated from the onset of the flash stimuli to this peak.

OPs were also analyzed as high-frequency components superimposed on the ascending limb of the b-wave, occurring between the a-wave trough and the b-wave peak. These fast wavelets are typically observed in the frequency range of 75–300 Hz. To characterize OPs more precisely, a complex Morlet wavelet

transform was applied to each trace (Righetti et al. 2025). The Morlet wavelet, defined as the product of a complex sinusoid and a Gaussian envelope, was convolved with the signal to produce a time–frequency representation. This transformation yielded a multi-dimensional map of the signal, in which frequency (Hz), time (ms), and power (dB) were extracted and visualized. Power values were normalized using a baseline division, enabling clearer interpretation of signal strength across time and frequency domains. The use of complex Morlet wavelets has previously been shown to improve the analysis of biological signals such as electroencephalography (Cohen 2019), and here it was similarly applied to enhance the characterization of ffERG responses. Time, frequency and power together with amplitude and implicit times of a- and b-waves of each subject and each eye were stored in a table and exported as .csv file.

Additionally, OPs traces were sub-filtered in three sets of frequency windows: 75-100 Hz, 100-150 Hz and 150-300 Hz. Time-series data from each subject were loaded and processed step-wise for each analysis stage. For each step and for both channels of interest (e.g., left and right eye), the corresponding signal and time vector were extracted. Signals were subjected to a series of band-pass filters defined by each set of frequency windows. For each frequency window, a finite impulse response (FIR) filter was designed using the least-squares method (*firls*) with a transition bandwidth of 10% around the passband. The filter order was determined as a function of the sampling frequency and the lower cutoff frequency, scaled by a factor of 3. This scaling factor was chosen empirically to balance filtering precision and signal smoothness. The filter was applied using zero-phase forward and reverse filtering (*filtfilt*) to avoid phase distortions. Filtered signals were stored for each subject, step, channel, and frequency band.

2.5 Statistical Analyses

To assess the effects of stimulus intensity and duration on OP features (frequency, latency, and power), statistical analyses were performed using Python (v3.12) and the *statsmodels*, *scipy* and *pingouin* packages. Prior to inferential testing, data distributions were checked for normality using the

Shapiro-Wilk test, and homogeneity of variances was assessed via Levene's test. Depending on the outcome of these preliminary checks, one of the following statistical approaches was applied: if assumptions of normality and equal variances were met, a two-way ANOVA was conducted, followed by Tukey's HSD post-hoc test for multiple comparisons. If the data were normally distributed but violated the assumption of equal variances, Welch's ANOVA was applied, followed by Games-Howell post-hoc comparisons. In cases where the assumption of normality was not satisfied, a Kruskal-Wallis test was performed separately for each factor, and, when significant, followed by Dunn's post-hoc test with Bonferroni correction. Statistical significance was set at a p-value lower than 0.05 for all tests.

3 Results

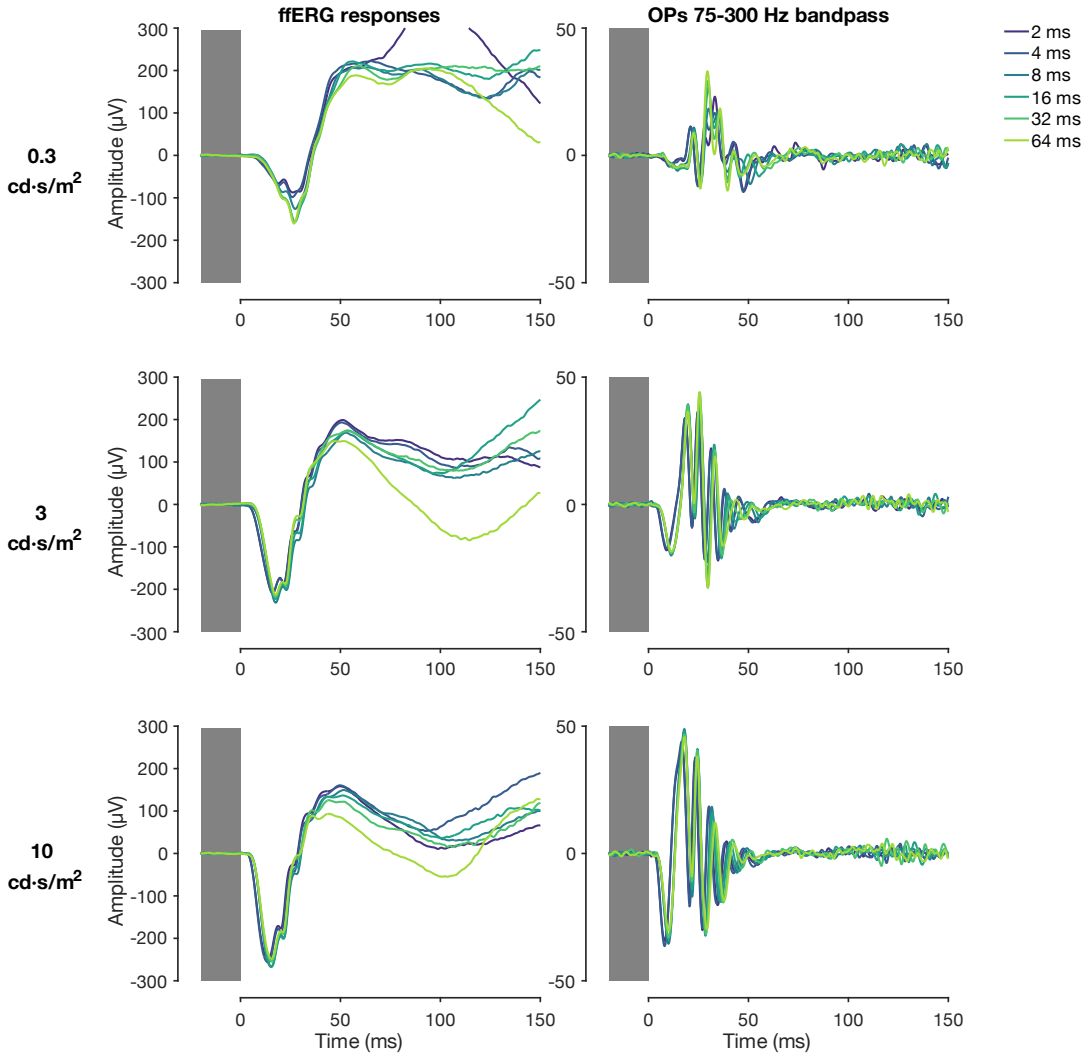

Figure 4 - ERG and OP Responses of all Durations

FfERG recordings of healthy subjects according to the protocol described in 2.3. The graphs show the amplitude (µV) on the y-axis and the time (ms) on the x-axis. In the left column, the averaged ERG responses of all subjects are shown. On the right, the plots show filtered OP traces (75–300 Hz) of the corresponding ERGs. Both columns are separated into three lines which show the different luminance levels 0.3 cd·s·m^{-2} , 3 cd·s·m^{-2} and 10 cd·s·m^{-2}, from top to bottom. The lines of different colours represent the various stimulus durations 2, 4, 8, 16, 32, 64 ms, ranging from dark blue portraying 2 ms to light green representing 64 ms duration, as indicated by the color key in the top right corner. The baseline period before stimulus onset (-20 to 0 ms) is indicated with the grey area.

3.1 Electrophysiological Results

Serving as an overview, Figure 4 shows the averaged raw ERG and filtered OP traces of all participants as well as all stimulus conditions included in the protocol.

3.1.1 ffERG Responses

The averaged raw ERG traces are shown in the left column of Figure 4. On the first row, the traces of the lowest luminance, 0.3 cd·s·m^{-2}, are displayed. They revealed a comparably low-amplitude a-wave. Among the a-wave amplitudes of different stimulus durations, an increase in amplitude from shorter to longer stimuli can be observed. Measured from the a-wave trough to the b-wave peak, the variability of b-wave amplitudes among the stimulus duration was within a small range. Indentations of the unfiltered OPs, referred to in Figure 3, which are to be expected on the ascending limb of the b-wave, were barely visible.

Below, there are the two higher luminance levels, 3 cd·s·m^{-2} in the second and 10 cd·s·m^{-2} in the third row. The amplitude of the a-wave increased with each luminance level, with 10 cd·s·m^{-2} evoking the highest a-wave amplitude. In the two higher luminance levels, the a-wave amplitude essentially did not vary among the stimulus durations. In the 3 and 10 cd·s·m^{-2} traces, the b-wave amplitude increased with increasing stimulus durations. The resulting gap between amplitudes of different durations increased from 3 to 10 cd·s·m^{-2}. In both recordings, the sawtooth-like pattern of the unfiltered OPs on the b-wave's ascension was clearly visible.

3.1.2 Filtered OPs

The OP traces resulting from applying a 75-300 Hz bandpass filter on the averaged raw ERG traces are shown in the right column of Figure 4. Comparing the 0.3 cd·s·m^{-2} responses to the 3 and 10 cd·s·m^{-2} traces, it possessed a considerably lower amplitude. Further, the pattern of the 0.3 cd·s·m^{-2} OPs diverged from those of the other luminance levels, since it lacked the initial steep trough and the following sharp OP peaks. Among different stimulus durations, the

patterns of the 0.3 cd·s·m^{-2} OPs diverged, leading to a diffuse overall pattern. In the two higher luminance levels' responses, the overview on the OP traces showed clearly delineated OP peaks, since the traces elicited by different stimulus durations exhibited a homogenous pattern. When examining individual OP peaks, their amplitudes varied both across different stimulus durations and across the two luminance levels.

3.1.3 Comparison of the 4 and 64 ms Responses

Figure 5 shows the averaged ffERGs and the extracted OPs corresponding to only two different stimulus durations. On the one hand, blue lines represent 4 ms stimulus duration, which is the standardly used duration for OP recordings. On the other, green lines indicate the longest stimulus used in this protocol, 64 ms. The comparison of these responses enabled a better illustration of the effects of altering the stimulus duration. Regarding the conventional ERG responses, it essentially confirmed the previous descriptions based on Figure 4.

Figure 5 revealed differences between OP traces of the two stimulus durations of the 0.3 cd·s·m^{-2} responses. The amplitudes of the 64 ms OPs exceeded those of the shorter duration so that the corresponding OP peaks could be defined more clearly. The patterns of the two durations' traces diverged, as well. Overall, the OPs of both durations of this luminance differed markedly from those of the higher luminance levels.

Apart from different amplitudes of individual OP peaks, the 3 and 10 cd·s·m^{-2} OPs featured resembling characteristics, when comparing the two illustrated stimulus durations. In both durations' responses, the initial three deflections were quite similar in appearance with only minor amplitude differences. Towards the later phase of the deflections, the responses diverged. Whilst in both luminance levels, there were only four clearly definable OP peaks in the 64 ms response, the traces evoked by 4 ms stimulus duration included five peaks. This additional ultimate peak was relatively small in both luminance levels.

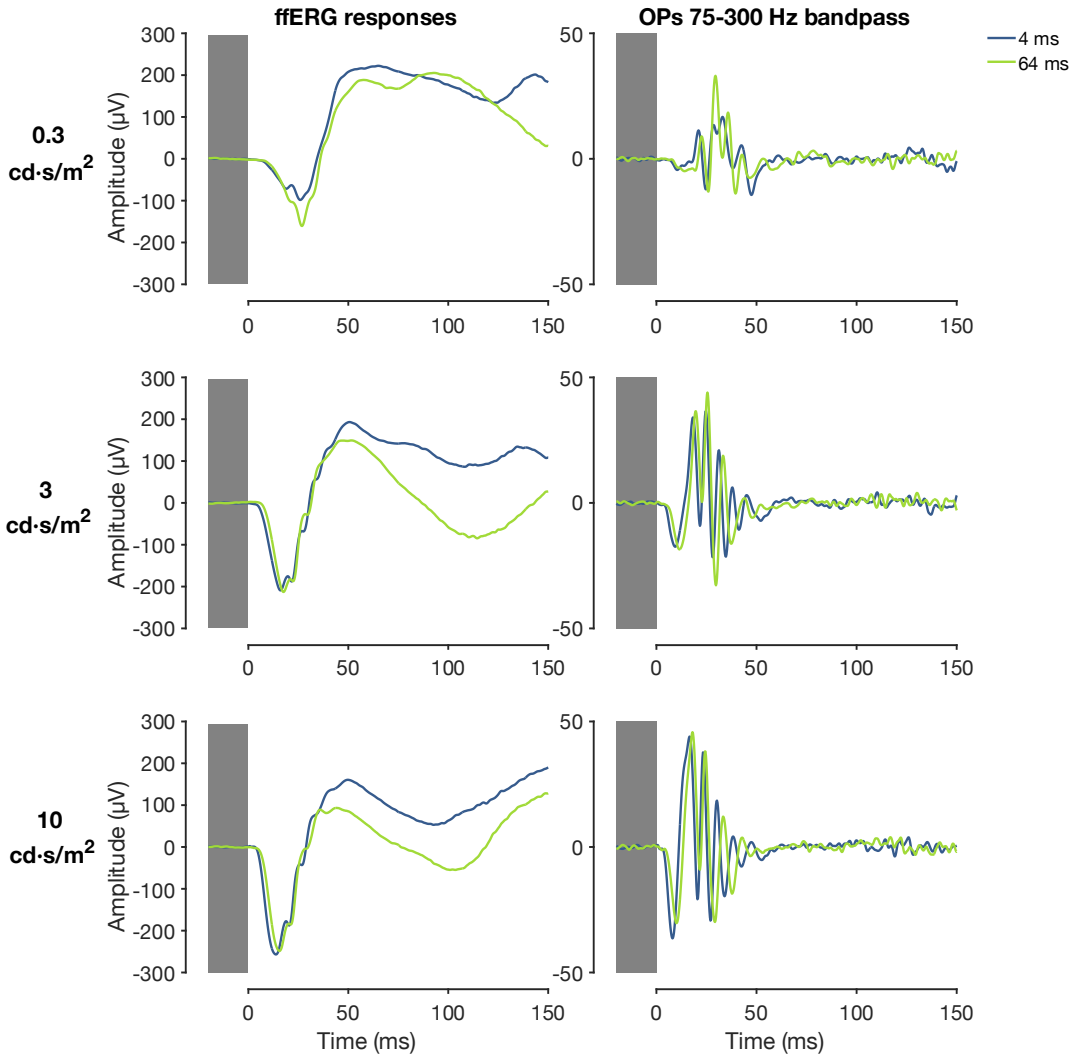

Figure 5 - Comparison of 4 and 64 ms ERGs and OPs

FfERG recordings of healthy subjects according to the protocol described in 2.3. The graphs show the amplitude (µV) on the y-axis and the time (ms) on the x-axis. In the left column, the averaged ERG responses of all subjects are shown. On the right, the plots show filtered OP traces (75–300 Hz) of the corresponding ERG. Both columns are separated into three lines which show the different light intensities 0.3 cd·s·m^{-2}, 3 cd·s·m^{-2} and 10 cd·s·m^{-2}, respectively. The lines of different colours represent stimulus durations 4 and 64 ms, with blue representing 4 ms and green representing 64 ms duration, as indicated by the color key in the top right corner. The baseline period before stimulus onset (-20 to 0 ms) is indicated with the grey area.

3.2 Statistical Evaluation

To visualize the quantitative parameters time, frequency and power of the recordings, these parameters were extracted from the point of maximal power of each step's recording. Therefore, Figure 6, Figure 7 and Figure 8 serve as illustrations for an enhanced comparison of the data. Testing performed to complement these illustrations is described in this section, as well.

3.2.1 Frequency

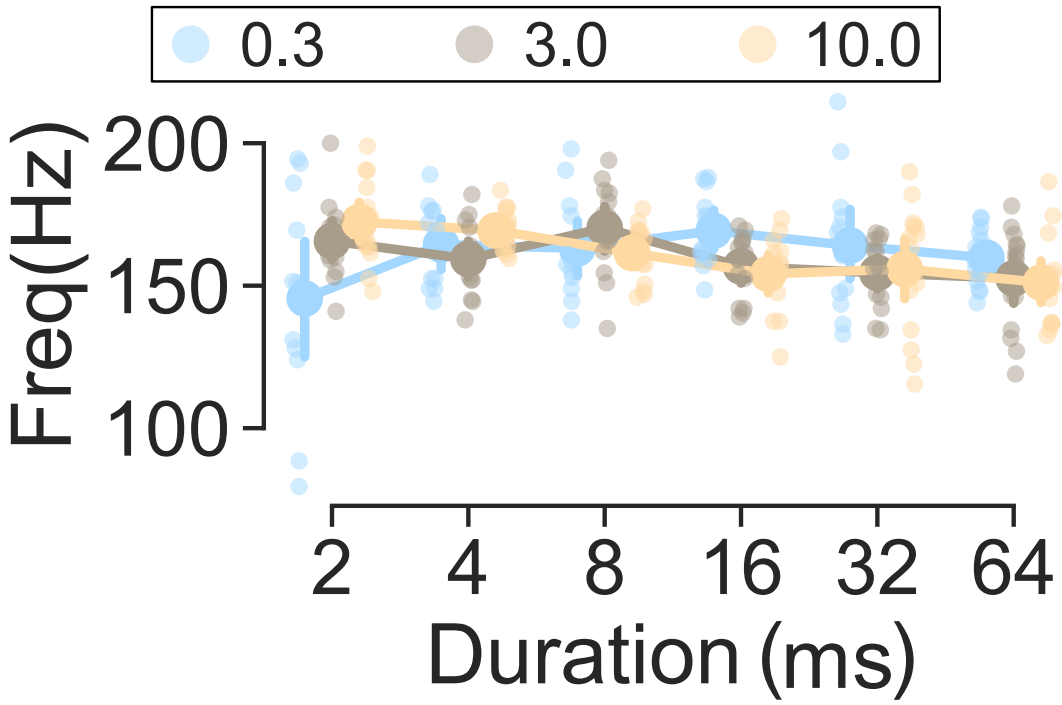

Figure 6 - Statistical Evaluation of Frequency
Illustration of the statistical evaluation of the frequency at maximal power of the recordings of each step in the protocol of the ffERG recordings. The data were extracted using a complex Morlet wavelet transform. On the y-axis, the Frequency in Hertz (Hz) is represented. The parameters refer to all six durations (ms) which are located on the x-axis. Different colors represent the three luminance levels: blue represents 0.3, brown represents 3 and yellow represents 10 cd·s·m^{-2}.

Regarding the frequency at to point of the highest power, all three luminance levels appeared to be quite homogenous, when looking at Figure 6 only. The figure also indicated that the frequency decreased slightly with increasing stimulus durations. To statistically examine these findings, a Welch ANOVA test

was performed, which revealed that the luminance in fact did not have a significant impact. For the stimulus duration, however, the results indicated a statistically significant effect ($F_{(5)}$ = 3.1991, p-uncorrected = 0.009). Thereafter, a Games-Howell's post-hoc test was performed to correct for multiple comparisons. The following comparisons were found to be statistically significant: 4 vs. 64 ms, p-value corrected 0.01236, 8 vs. 64 ms, p-value corrected 0.01979. This underlined the visually described tendency.

3.2.2 Timing

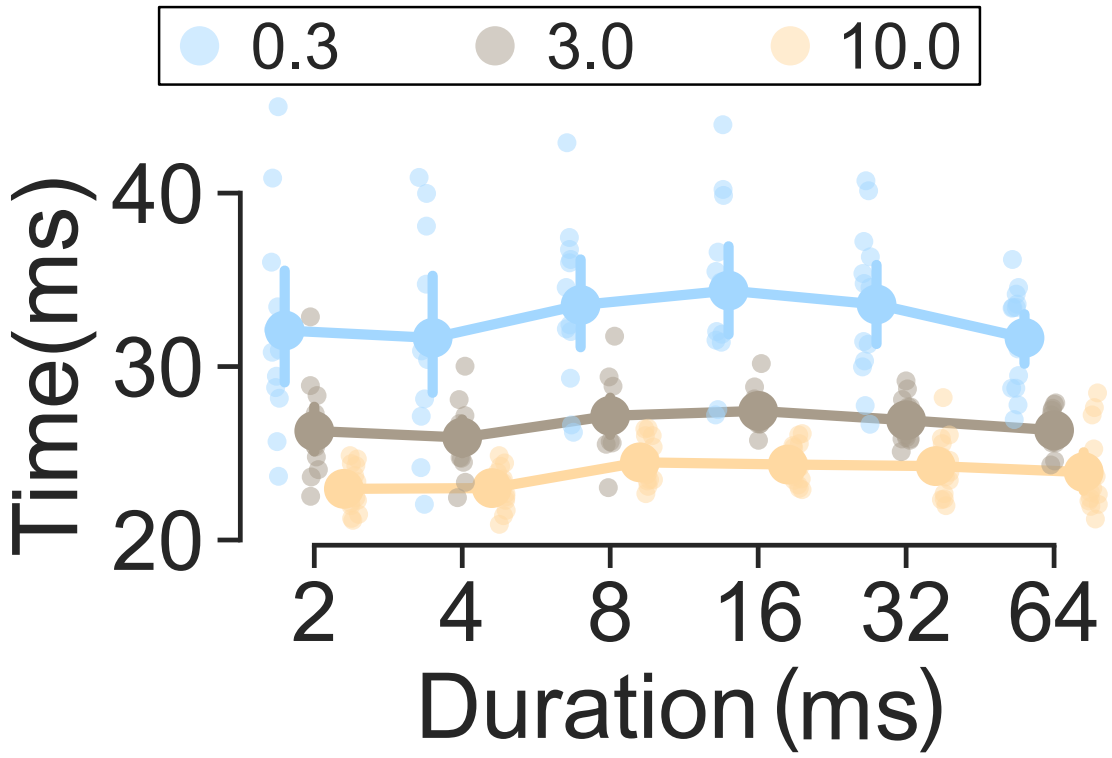

Figure 7 - Statistical Evaluation of Timing
Illustration of the statistical evaluation of the timing at maximal power of the recordings of each step in the protocol of the ffERG recordings. The data were extracted using a complex Morlet wavelet transform. On the y-axis, the time (ms) is represented. The parameters refer to all six durations (ms) which are located on the x-axis. Different colors represent the three luminance levels: blue represents 0.3, brown represents 3 and yellow represents 10 cd·s·m^{-2}.

Figure 7 allows an assessment of the timing at which the power reached its maximum in the respective step. The three curves corresponding to the three luminance levels appeared visibly separate from each other, implying that there

were differences in timing when different luminance levels were involved. The bottommost, which means that the corresponding measurements had the shortest interval to stimulus onset, of these curves represented the highest luminance, 10 $cd \cdot s \cdot m^{-2}$. The second highest luminance's maximum power appeared only slightly later. However, with an interval to stimulus onset exceeding 30 ms, there was a substantial gap between the timing of the 0.3 $cd \cdot s \cdot m^{-2}$ response maximum and those of the other luminance levels. As opposed to the differences between the luminance levels, the graph indicated that varying the duration did not influence the timing of the maximum power. To assess the timing, a Kruskal-Wallis test was performed to assess the significance of both duration and luminance. The results suggested that only the luminance was statistically significant ($H_{(2)}$= 162.841, p-uncorrected = 4.358e-36). The consequently performed Dunn's post-hoc test, to correct for multiple comparisons, revealed that all the luminance comparisons showed significant differences: 0.3 vs. 3, p-value corrected < 0.0001, 0.3 vs. 10, p-value corrected < 0.0001 and 3 vs. 10, p-value corrected < 0.0001.

3.2.3 Power

Figure 8 shows the maximum powers of each of the steps. The averaged values of all three luminance levels were located within the range between 20 and 30 dB. Nevertheless, the 0.3 $cd \cdot s \cdot m^{-2}$ response deviated from the other two luminance levels. Between the power of the 3 and 10 $cd \cdot s \cdot m^{-2}$ responses, the graph showed only a marginal difference with the brown line reaching slightly higher levels. An influence resulting from different stimulus durations could not be derived from the graph. To assess the significance of the effect of both duration and luminance, a Kruskal-Wallis test was performed. The results indicated that only the luminance caused a statistically significant difference ($H_{(2)}$ = 34.49, p-uncorrected = 3.23e-08). Subsequently, a Dunn's post-hoc test was performed, to correct for multiple comparisons. The following comparisons were found to be statistically significant: 0.3 vs. 3, p-value corrected < 0.0001, 0.3 vs 10, p-value corrected < 0.0001.

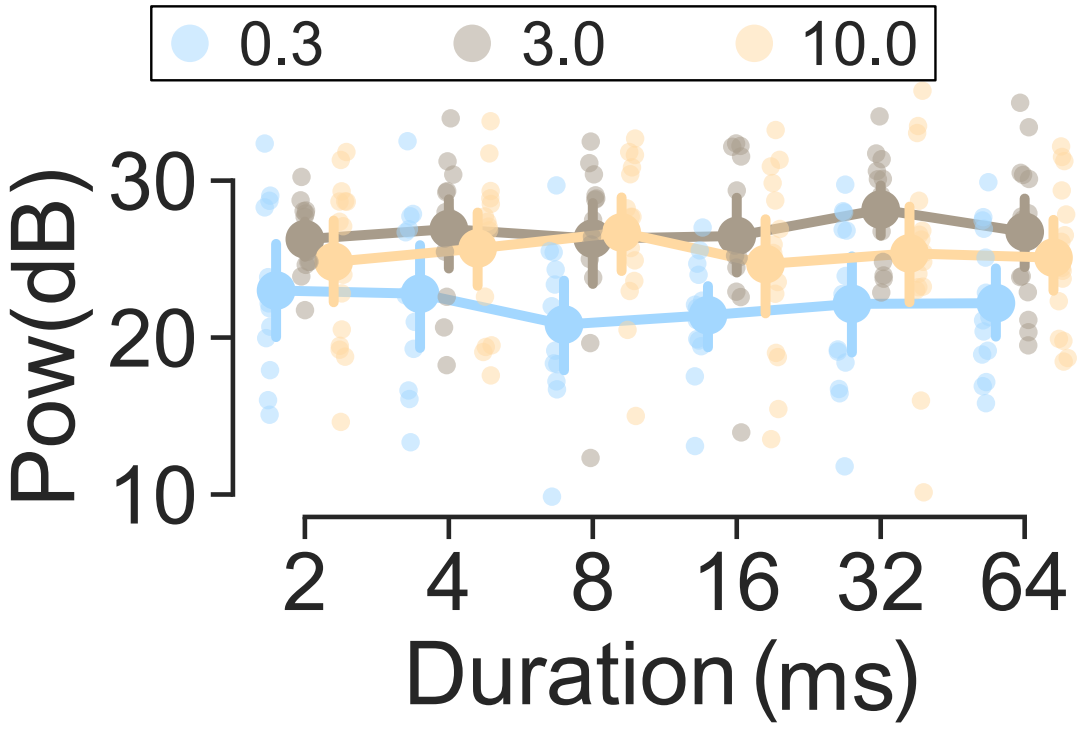

Figure 8 - Statistical Evaluation of Power
Illustration of the statistical evaluation of the maximal power of the recordings of each step in the protocol of the ffERG recordings. The data were extracted using a complex Morlet wavelet transform. On the y-axis, the Power (dB) is represented. The parameters refer to all six durations (ms) which are located on the x-axis. Different colors represent the three luminance levels: blue represents 0.3, brown represents 3 and yellow represents 10 cd·s·m^{-2}.

3.3 Complex Morlet Wavelet Transform

The scalograms which are displayed in Figure 9 resulted from applying a complex Morlet wavelet transform to the measured ffERG traces. Utilizing this method, three parameters, frequency, time and relative power, were exhibited at the same time.

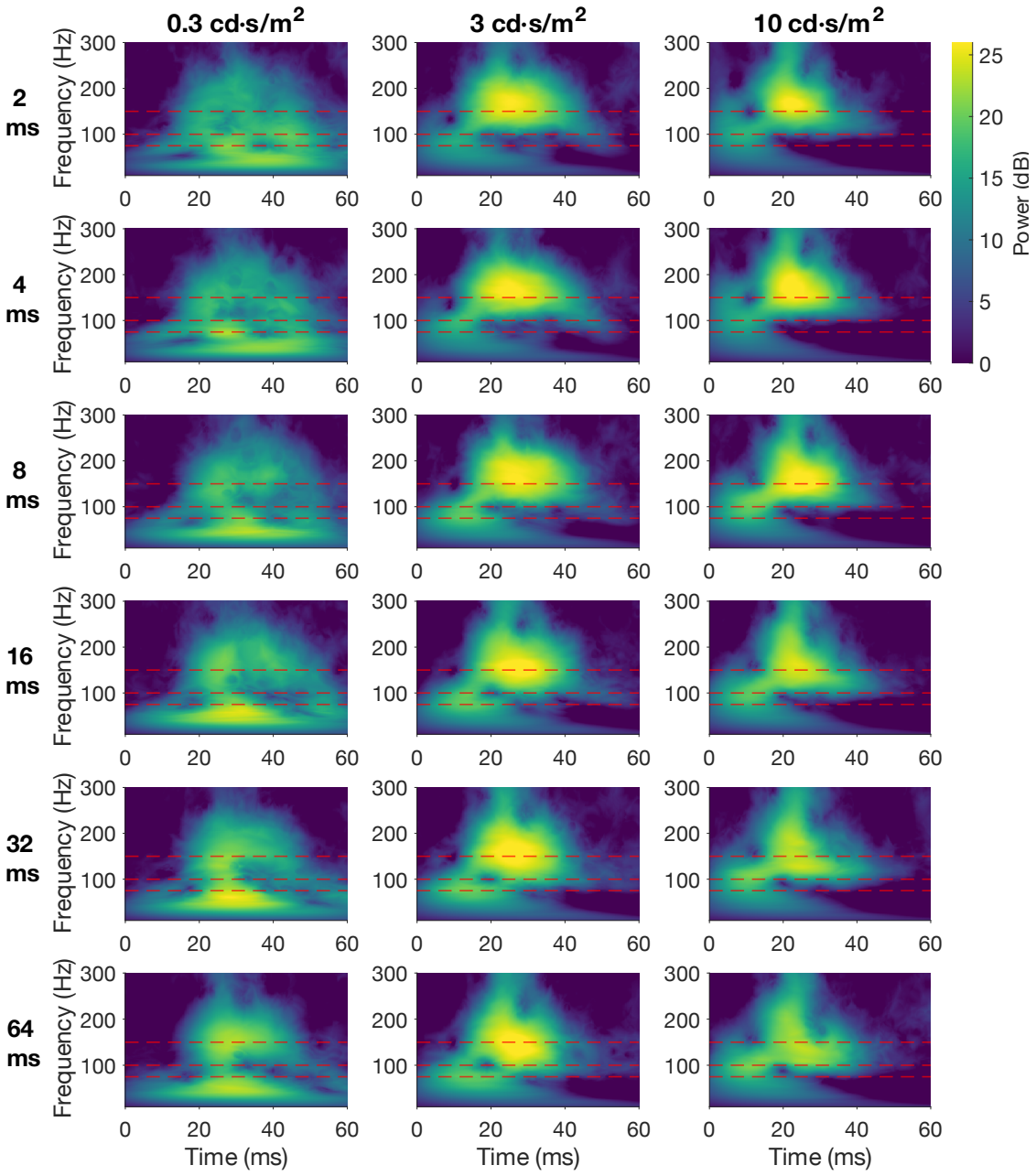

Figure 9 - Morlet Wavelet Transform Scalograms of all Recordings

Illustration of Morlet wavelet transform scalograms of all the steps used in the protocol. The scalograms show relative power (dB) in relation to frequency (Hz) on the y-axis and time (ms) on the x-axis. The relative power is displayed by a spectrum of colors ranging from dark blue, which represents low power up to yellow as the strongest power recorded, as illustrated by the color bar on the top-right. The three luminance levels are separated into columns which show, from left to right, 0.3, 3 and 10 cd·s·m^{-2}. From top to bottom, the six durations are arranged in lines from the shortest to the longest duration. For each panel, three red dashed lines are displayed at the level of 75, 150 and 300 Hz, indicating frequency windows used in the subsequent analysis.

3.3.1 0.3 cd·s·m^{-2} Scalograms

In the left column, all the scalograms which belong to the lowest luminance can be observed. Starting with the shortest duration in the top left corner, the relative power appeared to be distributed broadly over an area ranging between 10 and 60 ms with a frequency range from 10 to 250 Hz. Within this area a single main cluster mostly below a frequency of 50 Hz could be identified. Above 50 Hz, the relative power was dispersed without a clear pattern. For the most part, this description could be applied to the 4 ms scalogram apart from an additional small cluster which demarcated itself around 25 ms after stimulus onset at 75 Hz. With the step to 8 ms stimulus duration, the power concentrated increasingly between 20 and 40 ms after stimulus onset. This concerned both the previously described main cluster and the frequencies above it, so that a cluster at 150 Hz between 20 and 40 ms delimited itself. At 16 ms stimulus duration, the main cluster increasingly condensed with its maximum being located between just below 75 Hz at 30 ms. Concentration of power between 20 and 40 ms further increased at 32 ms stimulus duration, associated with a better demarcation of the high-frequency cluster and a frequency band connecting the two clusters at 30 ms latency. The division into two clusters became more evident in the longest duration's scalogram: because of a reduced concentration of the lower-frequency alongside the increasing power of the high-frequency cluster, both appeared equally powerful in this duration.

3.3.2 3 cd·s·m^{-2} Scalograms

The scalograms resulting from 3 cd·s·m^{-2} stimulus intensity are displayed in the middle column. At 2 ms stimulus duration, there was a powerful cluster between 100 and 250 Hz, which had its center around 175 Hz. This cluster occurred between 20 and 40 ms. Prior to this leading cluster, only shortly after stimulus onset, another, less powerful cluster could be defined between 75 and 100 Hz. Both clusters appeared connected by a branch at 125 Hz. At about 10 ms after stimulus onset, a "hole", i.e. a small area with especially low power at a frequency just below 150 Hz, appeared. The frequency, at which this "hole" appeared,

slightly increased to 150 Hz at 8 ms stimulus duration, remaining there for the rest of the protocol. 8 ms stimulus duration elicited a broader, i.e. longer small cluster. It prolonged further in the following durations' scalograms, forming a second interconnection to the main cluster between 75 and 100 Hz. Between the two clusters and their interconnections, another low-power area or "hole" appeared at 100 Hz, 20 ms after stimulus onset. The main cluster remained essentially constant in the responses to 2, 4 and 8 ms stimulus duration. In the 16 ms scalogram, the frequency, at which the main cluster's center appeared, decreased to 150 Hz. This dominant frequency further declined, so that the main cluster's center was majorly located below 150 Hz in the 64 ms stimulus duration scalogram. In the earlier half of the cluster, a frequency band reaching up to 300 Hz emerged and became more powerful in the response to the subsequent stimulus durations. Conversely, the power above 150 Hz gradually decreased in the second half of the main cluster between the responses to 8 and 64 ms stimulus duration.

3.3.3 10 cd·s·m^{-2} Scalograms

The column on the right offers an overview of the 10 cd·s·m^{-2} scalograms. As in the intermediate luminance, the scalogram featured two clusters. An earlier cluster characterized by its small size and low power appeared shortly after stimulus onset between 75 and 125 Hz. The second and main cluster occurred around 25 ms after stimulus onset. The main cluster majorly appeared at a frequency between 100 and 200 Hz, with its center just above 150 Hz. In the earlier part of the cluster, a thin frequency band reached up to 300 Hz. Comparable to the previous luminance, there was a "hole" at 150 Hz, 10 ms after stimulus onset, which maintained these attributes in all 10 cd·s·m^{-2} scalograms. Regarding the development between the 2 and 8 ms stimulus duration scalograms, merely the power of the early cluster increased. At the transition from 8 to 16 ms duration, the main cluster changed remarkably due to a general decrease of power. Particularly, the power in the later phase of the cluster at frequencies above 150 Hz diminished, while the frequency band in the early

phase of the cluster, reaching up to 300 Hz, remained intact. The loss of power also manifested as a reduced maximal power in the center, causing a large part of the cluster's power to shift below 150 Hz. These developments continued in the responses to the two longest stimulus durations, so that the main cluster of the 64 ms scalogram consisted of a higher-frequency part at 25 ms and a broad, lower-frequency part between 75 and 150 Hz from 20 to 40 ms after stimulus onset. At 20 ms between 75 and 100 Hz, a second "hole" with diminished power appeared.

3.3.4 Detailed Comparison of 4 ms and 64 ms Scalograms

Figure 10 displays the scalograms of the standard stimulus duration, 4 ms, and the longest stimulus duration utilized, 64 ms, respectively for the three luminance levels. This enabled a better visual comparison of the effects of varying stimulus duration. When examining the differences in the scalograms across the three luminance levels, clear distinctions in the distribution of power could be observed between 0.3 $cd \cdot s \cdot m^{-2}$ and the two higher luminance levels. Particularly in the response to 4 ms stimulus duration, the power in the lowest luminance condition was distributed over a broad range. The 0.3 $cd \cdot s \cdot m^{-2}$ scalograms exhibited relatively high power in the frequency range below 50 Hz compared to the higher luminance levels. While the latter were essentially terminated by 40 ms after stimulus onset, the 0.3 $cd \cdot s \cdot m^{-2}$ scalograms still showed residual power beyond 40 ms. Due to the cluster around 150 Hz, the scalogram of the longer stimulus duration at the lowest luminance partly resembled that of the higher luminance levels, in which the main cluster in this range was characteristic. However, the higher luminance levels additionally exhibited the earlier cluster described above. Another distinguishing feature was the presence of the described "holes", which were similarly located in the two higher luminance levels but were not as remarkable in the scalograms of the lowest luminance.

Comparing the effect of prolonging the stimulus duration, Figure 10 revealed that it varied depending on the applied luminance. Given the distinct appearance of the 0.3 $cd \cdot s \cdot m^{-2}$ scalograms, the effect of prolonging the stimulus duration was

not amenable to comparison. Essentially, it resulted in a concentration of power on two clusters at 30 ms after stimulus onset in the 0.3 cd·s·m^{-2} scalograms.

In the 3 and 10 cd·s·m^{-2} scalograms, both luminance levels shared a few common effects caused by the increased stimulus duration. The power of the early cluster increased from 4 to 64 ms stimulus duration. The power of the main cluster shifted towards lower frequencies. Above 150 Hz, the development of the main cluster diverged into an early and a later component relative to stimulus onset. In the early component, a frequency band extending up to 300 Hz became more pronounced. In the later component, a reduction in power occurred. This reduction was most prominent at the highest luminance level, where a very marked decrease in power manifested in this area (Righetti et al. 2025).

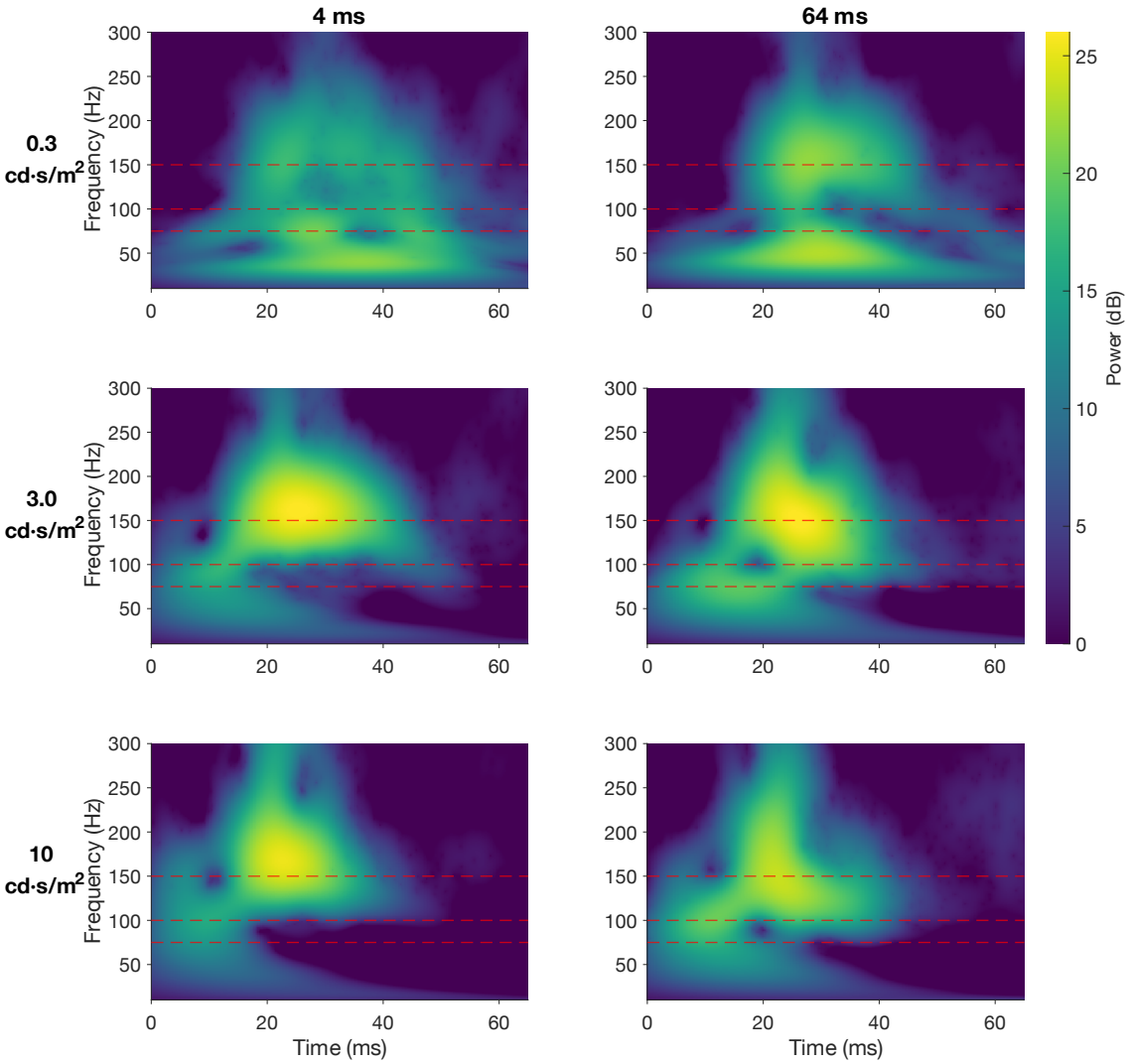

Figure 10 - Comparison of 4 and 64 ms Scalograms
Illustration of Morlet wavelet transform scalograms of the stimulus durations 4 and 64 ms for each of the three luminance levels, respectively. The scalograms show relative power (dB) in relation to frequency (Hz) on the y-axis and time on the x-axis. The relative power is displayed by a spectrum of colors ranging from dark blue, which represents low power up to yellow as the strongest power recorded, as illustrated by the color bar on the top-right. The three luminance levels are separated into lines which show, from top to bottom, 0.3, 3 and 10 cd·s·m^{-2}. The columns represent the stimulus durations with 4 ms on the left and 64 ms on the right. For each panel, three red dashed lines are displayed at the level of 75, 150 and 300 Hz, indicating frequency windows used in the subsequent analysis.

3.4 Frequency-Specific Filtering

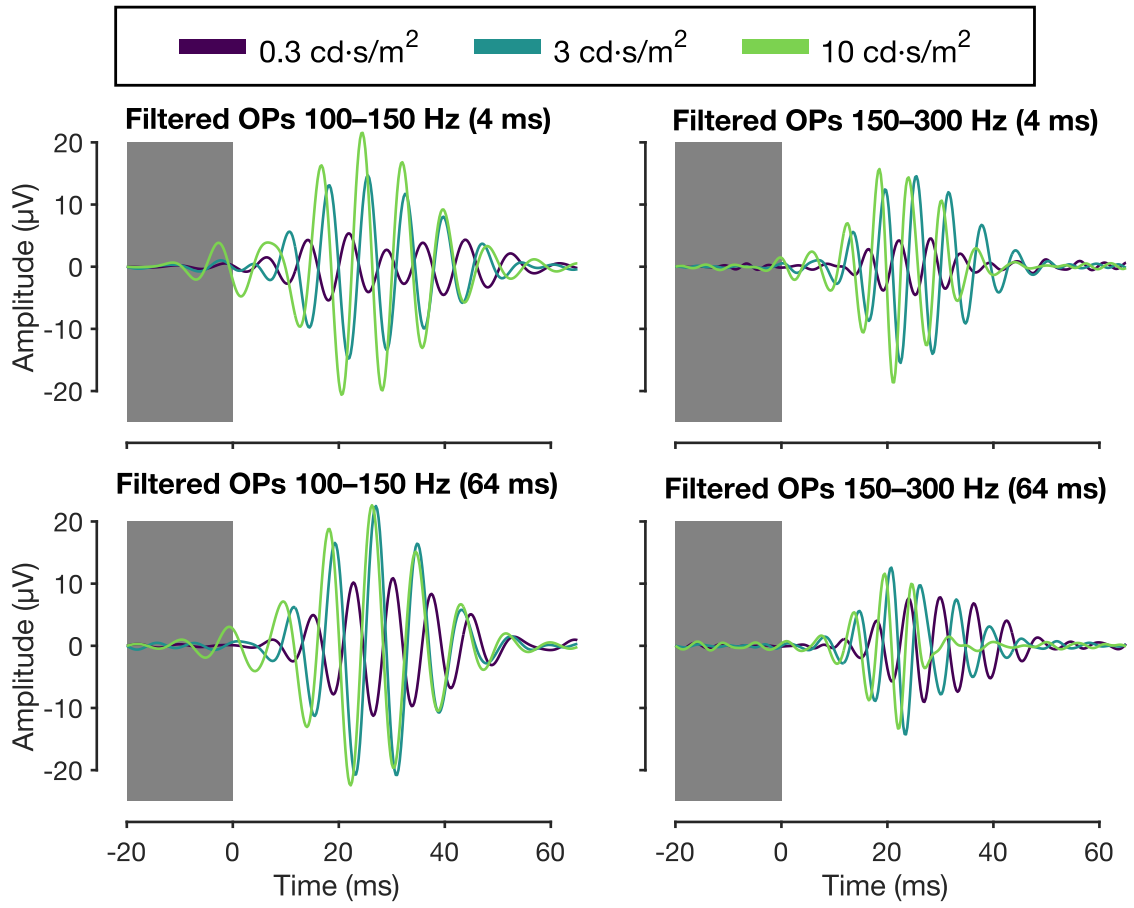

Figure 11 - Frequency-specific Filtering
OP traces resulting from differentially filtering the ffERG responses evoked by using stimulus durations of 4 and 64 ms. The graphs show the amplitude (µV) on the y-axis and the time (ms) on the x-axis. Different colors are utilized to illustrate the three different luminance levels: purple traces represent 0.3 cd·s·m^{-2}, turquoise traces 3 cd·s·m^{-2} and green traces 10 cd·s·m^{-2}. The figure is separated into two frequency-specific filters: frequencies from 100-150 Hz on the left and frequencies from 150-300 Hz on the right. Responses to 4 ms stimulus duration are shown in the upper row, those to 64 ms stimulus duration in the lower row. The baseline period before stimulus onset (-20 to 0 ms) is indicated with the grey area.

With the complex Morlet scalograms showing changes over different durations especially in the higher frequency spectrum, the OP traces were filtered regarding their frequencies to scrutinize their behavior within selective frequency windows. This was achieved by applying a bandpass filter to extract three frequency windows. The lowest frequency window ranged from 75 to 100 Hz, the intermediate filter covered 100 to 150 Hz whilst the highest frequency window reached up to 300 Hz. Figure 11 shows the results from this differential filtering.

In the top line, it displays the response to 4 ms stimulus duration. In the bottom line, the curves resulting from the protocol's highest stimulus duration, 64 ms, are shown. For both durations, the left part displays the intermediate, the right part the high frequency filter, respectively.

3.4.1 Filtered Responses to 4 ms Stimulus Duration

In the intermediate frequency window of 4 ms stimulus duration displayed in the top left, the purple-colored curve resulting from 0.3 $cd \cdot s \cdot m^{-2}$ differed considerably from the other two curves. All of its deflections were within a tight, very low-amplitude range. In contrast, the turquoise, representing 3 $cd \cdot s \cdot m^{-2}$, and green trace, representing 10 $cd \cdot s \cdot m^{-2}$, shared a similar fusiform shape. In both high-luminance levels, the OP amplitudes noticeably exceeded the blue curve's amplitudes. Within both high-luminance traces, four major positive-going OP deflections were evoked. They were accompanied by lower deflections preceding and following the major peaks, which complemented the fusiform shape.

The curves displayed in the top right graph derived from applying the filter for the highest frequency window (150-300 Hz) on responses resulting from the same conditions as in the previous section. Although resembling a fusiform shape as opposed to its counterpart on the left, the 0.3 $cd \cdot s \cdot m^{-2}$ curve's amplitude remained much lower than that of the other two curves. The 3 $cd \cdot s \cdot m^{-2}$ response in the high frequency window essentially possessed the same configuration and matched the amplitude of the response in the intermediate window. The green 10 $cd \cdot s \cdot m^{-2}$ trace, in contrast to the turquoise trace, appeared heterogenous in the altering frequency filters. Overall, its amplitude was almost globally lower. The major OPs were differentially affected by this reduction. The first major OP's amplitude remained relatively constant. The second OP's amplitude decreased markedly. Whereas the second OP's amplitude still exceeded the corresponding 3 $cd \cdot s \cdot m^{-2}$ OP, the third fell below the turquoise response. The most distinct reduction occurred to the last major OP and the following deflection, which were diminished to the level of the 0.3 $cd \cdot s \cdot m^{-2}$ response.

3.4.2 Filtered Responses to 64 ms Stimulus Duration

The responses elicited by 64 ms stimulus duration are displayed in the lower section of Figure 11. Regarding the 0.3 cd·s·m^{-2} response, unlike 4 ms stimulus duration, 64 ms evoked a curve with a fusiform shape, comparable to the stronger stimuli, in the intermedium frequency window. In the same window, with respect to 4 ms stimulus duration, all stimulus intensities at 64 ms duration elicited more powerful responses. Consequentially, in the 0.3 cd·s·m^{-2} response to this duration, four major OPs resembling those evoked by the higher luminance levels emerged. Regarding both higher luminance levels, the amplitude increase from 4 to 64 ms duration was more pronounced in the 3 cd·s·m^{-2} response, so that it approached the 10 cd·s·m^{-2} line, thus looking almost identical to it. All deflections of these two responses, like in the previous graphs, exceeded the corresponding deflections in the lowest luminance. They shared the fusiform shape seen in the previously describes graphs.

Scrutinizing the 64 ms response between 150-300 Hz, the following aspects could be observed. Referring to the intermediate frequency window, the power in all luminance levels' responses decreased. The waveform of the 0.3 cd·s·m^{-2} response was least affected. Moreover, its amplitudes were larger than in the 4 ms response in the corresponding frequency window. The amplitudes of the major OPs of the 3 cd·s·m^{-2} response were unequally decreased compared to the corresponding OPs in the intermediate frequency window. In relation to the other OPs, the amplitude decrease least affected the first major OP. Both the third and the fourth wavelet reduced below their 0.3 cd·s·m^{-2} counterparts, the latter even close to baseline level. Including the first two major OPs, the course and amplitude of the responses to 3 and 10 cd·s·m^{-2} in the high frequency window were comparable. However, after the second major OP, the 10 cd·s·m^{-2} response was severely altered due to a sudden diminution of power (Righetti et al. 2025). Following the second major OP, there were only tiny deflections not distinguishable from the baseline noise. Therefore, they could not be reliably assigned to the remaining major OPs expected at this point, leaving the impression of a response terminated between 20 and 30 ms after stimulus onset.

3.5 Summary of the Results

The conventional ERG responses revealed that the a-wave's amplitude grew with increasing stimulus intensities. Varying the stimulus duration did not have a substantial effect, however. For the b-wave, these relations were essentially vice versa because the luminance levels did not cause major changes to the amplitude, whilst shorter elicited larger amplitudes than longer stimulus durations. The OPs extracted from the ERG responses revealed similar waveforms in the 3 and 10 $cd \cdot s \cdot m^{-2}$ responses, which differed from the 0.3 $cd \cdot s \cdot m^{-2}$ responses. In the latter, prolonging the stimulus duration increased the OP amplitudes. In the other luminance levels' OPs, the duration only had a minor impact on the amplitude. Their OP waveform remained consistent throughout all durations.

Statistical analyses were conducted for the parameters frequency, timing and power extracted using a complex Morlet wavelet transform. Whilst there were no significant frequency differences between luminance levels, 64 ms duration elicited significantly lower frequencies than 4 and 8 ms, respectively. The parameters timing and power were not influenced by stimulus duration as opposed to the significant differences between luminance levels.

In the illustrations resulting from applying a complex Morlet wavelet transform to the ERG traces, the 0.3 $cd \cdot s \cdot m^{-2}$ scalograms showed a distinct pattern with a low-frequency cluster and scattered power distribution above 75 Hz. With increasing stimulus durations, the latter concentrated to result in a second cluster at a higher frequency. In contrast, the 3 and 10 $cd \cdot s \cdot m^{-2}$ scalograms both contained a major cluster above 100 Hz and an earlier minor cluster around 100 Hz. Prolongation of the stimulus duration led to a decrease of the main clusters frequency and increase of the minor cluster's power in both higher luminance levels. Additional effects of the increased stimulus duration occurred in the major cluster's frequencies above 150 Hz (Righetti et al. 2025). They could be divided in two components. Within the early component, the cluster expanded towards higher frequencies, whereas in the later component, a loss of the cluster's power, especially in the 10 $cd \cdot s \cdot m^{-2}$ scalogram, was observed.

The frequency-specific filtering of the ERG responses also exhibited a distinct response to the lowest luminance. Its responses included substantially lower amplitudes and partly a deviant waveform. Extension of the stimulus duration increased the amplitudes of the 0.3 cd·s·m^{-2} OPs in both displayed frequency windows. In the higher luminance levels, the OPs elicited by 64 ms stimulus duration were larger in the intermediate but smaller in the high frequency filter, compared to those elicited by 4 ms. Most importantly, the high frequency filter to 64 ms stimulus duration revealed particularly reduced later OPs in both high luminance levels, most notably for 10 cd·s·m^{-2} (Righetti et al. 2025).

4 Discussion

4.1 Relating the Results to the OFF-pathway

When assessing the influence of the OFF-pathway, one should scrutinize the effect of modifying the stimulus duration on the OPs. The various methods used for the analysis of the responses to the stimuli applied during the protocol offered different perspectives. As the 3 and 10 $cd \cdot s \cdot m^{-2}$ responses showed the most important findings but differed markedly from the 0.3 $cd \cdot s \cdot m^{-2}$ responses, the latter will be referred to separately. The OP responses resulting from using the standard bandpass filter did not indicate a considerable influence of the OFF-pathway. The consistency of the OP waveforms between different durations emphasizes this most. The observed variance of amplitudes caused by duration changes, was quite unspecific and did not show a certain pattern. One could argue that the additional fifth OP-like deflection, which only appeared in the 4 ms but not in the 64 ms responses, could be related to the OFF-pathway. However, its amplitude was relatively small and it did not match the findings provided by the other analyses, especially when comparing their respective timings.

These other methods offered the advantage of assessing the responses with respect to the frequency. Thereby, they revealed systematic differences between the standard 4 ms and the higher stimulus durations, which only occurred at higher frequencies above 150 Hz. Noticeable was the sudden drop of power in the later phase above 150 Hz in the 10 $cd \cdot s \cdot m^{-2}$, 64 ms scalogram. Corresponding to this was the diminished amplitude of the OPs subsequent to the second major OP in the equivalent frequency-specific filtered response. In combination, these findings in the late phase of the response could indicate an influence of the OFF-pathway. Whilst the described effect appeared like a termination of the OPs in the strongest luminance, it was not as pronounced in the 3 $cd \cdot s \cdot m^{-2}$ response. The comparably slight power or amplitude decreases may be attributed to the OFF-pathway in the intermediate luminance, as well. Though, the effect apparently was smaller than in the highest luminance. Another important finding which resulted from increasing the stimulus duration was the decrease of frequency. It was not only significant in the statistical analysis but

visible in the time-frequency maps, as well. Consequentially, it was also reflected in the power distribution of the frequency windows of Figure 11. Matching the previously described findings, this may as well be ascribed to the OFF-pathway's influence.

Considering the overt differences between the 0.3 cd·s·m^{-2} responses and those of the higher luminance levels, they are to be interpreted differentially. One should distinguish between differences of the response pattern in general and the changes induced by the increased duration. The former revealed that the respective stimuli evoked substantially different retinal reactions. Affected were power and amplitude, which were lower in the 0.3 cd·s·m^{-2} responses. But even more important were the divergencies among their shapes, including the uncharacteristic OP pattern, the incomparable time-frequency cluster distribution and the non-fusiform shape in the first intermediate-frequency filter response to 0.3 cd·s·m^{-2}. It is this aspect that questions the extent to which 0.3 cd·s·m^{-2} is capable of evoking proper OPs. Based on these findings, it only makes sense that increasing the stimulus duration did not change the responses in the same manner as in the higher luminance levels. In fact, the lowest luminance reacted quite contrarily to prolonging the stimulus duration, especially in the frequency domain. Its high frequency section received an increment, which was most evident in the frequency-specific filtering and also affected the late phase of the response in the time-frequency map.

4.2 Discussing the Extent of Influence of the OFF-pathway on OPs

The previous section provided evidence for the involvement of the OFF-pathway in the OPs. However, our results suggest that the contribution is confined to a small area of the OPs. One indicator can be derived from the lack of clear evidence for the OFF-pathway in the standard OP recordings. Rather, they appeared only above 150 Hz while lower frequencies remained unaffected. Moreover, the alterations were not consistent among the three luminance levels. In turn, this could indicate that the effect of the OFF-pathway exhibits a significant dependence on stimulus strength. Further, it can be stated that the influence of

the OFF-pathway focusses on the later phase of the OPs, as the noticeable features predominantly took place in the second part of the responses. Thus, these observations suggest that the OFF-pathway is unlikely to initiate or solely generate the OPs but instead exerts a predominantly modulatory influence (Righetti et al. 2025).

4.3 The Significance of the Results in Context of the Literature

4.3.1 Comparison of Evidence with the Results

The purpose of this section is to connect the observations of this study with the present evidence in literature. The finding of the OFF-pathway particularly affecting the late phase of the OPs is in agreement with pharmacological studies conducted by Wachtmeister using glycine (1980) and ethanol (1981b). Particular consideration should be given to the study conducted by Kojima and Zrenner (1978). Since it was conducted under physiological conditions, it lends itself well to be compared to the results of the present dissertation. Though, the different stimulus parameters utilized in their protocol, including adaptive illumination, luminance, durations and partly differing intervals, should be incorporated into the evaluation. An important finding of the study was the close connection between stimulus duration and the implicit time of the last OP, which the authors attributed to a possible reset function of the last OP. Our results, however, did not reveal a corresponding correlate. Moreover, their data implied an increased OFF-effect with shorter stimuli, which was consistent with findings by Best and Bohnen (1957). This would be compatible with our results, assuming that the longer stimulus duration produced a reduced OFF-effect, which in turn accounts for the loss of energy in the latter part of the response. The decrease of frequency of the main cluster following the prolongation of stimulus duration may be explained by stronger cone contribution, since the frequencies of cone-driven OPs were lower than those of rod-driven OPs, as revealed in a study by Lei et al. (2006).

To explain the aberrant responses to the lowest luminance, it is useful to clarify the stimulus conditions. The stimulus intensity 0.3 $cd \cdot s \cdot m^{-2}$ is situated close to the DA 0.01 ERG, which is too weak to stimulate the cone system (A. G. Robson

et al. 2022). As both other utilized luminance levels evoke mixed rod-cone responses, the lesser photoreceptor stimulation in the lowest luminance may suffice as an explanation for the significant differences between the responses. This applies especially to the differing OP waveforms since optimal OPs require mesopic conditions (Wachtmeister 1998). Furthermore, the opposite effects to increased duration, i.e. the differing OFF-pathway effects between 0.3 $cd \cdot s \cdot m^{-2}$ and the other intensities, might stem from the respectively activated rod pathways. Whereas in mesopic conditions, alternative pathways like the direct connection to OFF cone BCs play a more important role, the response to weaker stimuli mostly proceeds via RBCs (Pasmanter and Petersen-Jones 2022). This would underscore the contribution of the signaling via OFF-BCs for the OPs, which had already been proposed by Righetti et al. (2021). The varying magnitudes of the reactions to increased duration at the two standard light intensities employed for the OPs suggest that the contribution of the OFF-pathway is modulated by luminance.

Regarding the overall impact of the OFF-pathway on OPs, findings from a pharmacological study on rabbits by Dong et al. (2004) could be referenced for comparison. Though, their data indicated a rather small contribution without a pronounced effect on a particular part of the OPs, which diverges from the presented results. However, they also pointed out that the influence might differ with extended stimulus duration as their findings resulted from a short duration flash. Overall, the presented findings provided evidence for a modulatory contribution of the OFF-pathway on the OPs. They also demonstrated that this contribution would preferentially affect the OPs' later phase and vary with the luminance of the stimulus.

4.3.2 Comparability among Evidence

Considering the diversity of studies and respective findings around the OPs and the OFF-pathway might raise the question of how all these results can be correct and compatible at the same time. Therefore, this section scrutinizes the comparability and conditions of some exemplary studies.

Looking at one of the most recent and relevant studies performed by Haq et al. (2023), several differences to physiological human ERG recordings can be noticed. Their experiment, which revealed a close tie between the OPs and the AC network coupled by gap junctions, employed an adapted ERG protocol on the extracted retinas from both wild-type and mutant mice from, from which a µERG was recorded. Additionally, pharmacological agents were applied to selectively manipulate the retinal response. Through these measures, naturally, a detailed insight into the retina can be achieved. Simultaneously, there is the risk of an oversimplification in the representation of the complex neuronal processes within the retina. For instance, following extraction, the retinas utilized for the µERG recordings were deprived from all the extraretinal influence and physiological circulation.

Of course, animal experimentation is often employed in the research on OPs. However, it should be considered that interspecies variability in responses may occur. As an example, the study by Dai et al. (2017) observed differences to the b-wave and OPs of other studies, which were ascribed to differences between the rats utilized in their study to the mice of the other investigation. Moreover, Akula et al. (2007) revealed pronounced discrepancies between the power spectra of human and rat OPs alongside aberrant OP responses in a study on retinopathy of prematurity.

Pharmacologically altering OP responses as described in the example above is another commonly used method in research on OPs. Whilst pharmacological agents may enable conclusions on selective cell types, some limitations should be emphasized, as well. The effect of substances may vary as illustrated by variable OP responses after application of TTX, including complete abolishment (Haq et al. 2023), selective removal of late OPs (Dong et al. 2004) and slightly decreased OPs with prominently delayed time-to-peak (Dai et al. 2017). Dong et al. (2004) argued that the selective reduction of late OPs by glycine blocker strychnine (Wachtmeister 1980) could be attributed to high strychnine doses and nonspecific action. Especially the latter must be considered in retinal studies since glycinergic transmission affects BCs, GCs and ACs (Wässle et al. 2009).

Naturally, many other neurotransmitters are not confined to a singular cell type or synapse, either.

The study presented in this dissertation can be considered a physiological study. As the recordings were performed on healthy human subjects, direct conclusions to the human retinal physiology can be drawn. The clearly structured protocol modeled on the ISCEV ffERG standard (A. G. Robson et al. 2022) enables optimal reproducibility. Limitations of the study comprise missing photopic responses and a small sample size. A general limitation of physiological studies is that they typically permit the derivation of theoretical conclusions yet cannot demonstrate a direct connection to a particular structure.

4.3.3 Future Perspective

As described at the outset, OPs remain the subject of intensive research in retinal electrophysiology. Meanwhile, several compelling theories and pieces of evidence have emerged regarding the cellular mechanisms underlying their generation. However, these findings are partly contradictory, not least because of the different research methods applied. Consequently, further studies are necessary to determine their origin unambiguously. The results presented in this work suggest the involvement of the OFF-pathway, while also pointing toward the need for additional investigations. In particular, the observed variability in the OFF-pathway's contribution merits closer examination, which could be achieved by conducting studies with similar stimuli but under photopic conditions. Since the key effects in this study became most apparent in the frequency-specific analyses, it would also be valuable to apply the analytical approaches described here in future research. As mentioned in the previous section, it would furthermore be advisable to perform studies under conditions that more closely approximate physiological reality, thereby allowing for more direct inferences into processes in the human retina.

5 Conclusion

Human OPs are a group of high-frequency, low-amplitude wavelets superimposed on the ascending limb of the b-wave of the ffERG. Therefore, a bandpass filter between 75–300 Hz is required to properly isolate them. Despite extensive research, the cellular origin of OPs remains unresolved, with a potential contribution by the OFF-pathway being debated.

The present study investigated the extent to which the OFF-pathway contributes to OPs. FfERG measurements were obtained from 15 participants. The ffERG protocol was adapted from the ISCEV standard protocol, with particular emphasis on systematically increasing the stimulus duration in several steps. In addition to standard extractions, the measurements were analyzed using a complex Morlet wavelet transform and frequency-specific filtering. The results revealed a reduction in energy, particularly in later response components and in higher-frequency ranges of responses to higher luminance levels and longer stimulus durations compared with the standard duration. This effect was most pronounced at the highest luminance.

Altogether, it can be concluded that the findings provided evidence for a likely influence of the OFF-pathway on OPs. Since the observed effects were limited to a specific range, a modulatory function of the OFF-pathway can be assumed. Furthermore, the influence of the OFF-pathway showed variability with respect to the applied luminance.

6 Deutsche Zusammenfassung

Die menschlichen oszillatorischen Potentiale sind eine Gruppe von Wellen mit hoher Frequenz und niedriger Amplitude, die auf den aufsteigenden Ast der B-Welle des Ganzfeld-ERGs aufgelagert sind. Daher ist ein Bandpass-Filter zwischen 75-300 Hz notwendig, um sie optimal darzustellen. Die zelluläre Herkunft der oszillatorischen Potentiale ist trotz umfassender Forschung noch ungeklärt, wobei eine Beteiligung des OFF-Pathways diskutiert wird.

Die vorliegende Studie beschäftigte sich mit der Frage, inwiefern der OFF-Pathway an den oszillatorischen Potentialen beteiligt ist. Dazu wurden Ganzfeld-ERG-Messungen an 15 Versuchspersonen durchgeführt. Die Ganzfeld-ERG-Messungen wurden von den ISCEV Standardprotokollen adaptiert, wobei insbesondere eine Steigerung der Reizdauer in mehreren Schritten Teil des Protokolls war. Die Messungen wurden, zusätzlich zu den standardmäßigen Extraktionen, mithilfe eines Complex Morlet Wavelet Transforms und Frequenz-spezifischer Filterung analysiert. Hierbei zeigte sich insbesondere im späten Teil und im Bereich hoher Frequenzen der Antworten höherer Lichtstärken bei längerer Reizdauer eine Reduktion der Energie im Vergleich zu der standardmäßigen Reizdauer. Diese war in der höchsten Lichtstärke besonders stark ausgeprägt.

Aufgrund der geschilderten Ergebnisse lässt sich abschließend konstatieren, dass ein Einfluss der OFF-Pathways auf die oszillatorischen Potentiale wahrscheinlich ist. Da die genannten Auffälligkeiten auf einen bestimmten Bereich begrenzt waren, ist von einer modulatorischen Funktion des OFF-Pathways auszugehen. Der Einfluss des OFF-Pathways zeigte außerdem eine Variabilität in Bezug auf die applizierte Lichtstärke.

7 References

Akula, J. D., et al. (2007), 'The oscillatory potentials of the dark-adapted electroretinogram in retinopathy of prematurity', *Invest Ophthalmol Vis Sci,* 48 (12), 5788-97.

Armington, John C. (1988), 'Electroretinogram, Electroretinography', *Sensory System I: Vision and Visual Systems* (Boston, MA: Birkhäuser Boston), 21-22.

Awatramani, G., Wang, J., and Slaughter, M. M. (2001), 'Amacrine and ganglion cell contributions to the electroretinogram in amphibian retina', *Vis Neurosci,* 18 (1), 147-56.

Ba-Ali, S., et al. (2022), 'Full-field and multifocal electroretinogram in non-diabetic controls and diabetics with and without retinopathy', *Acta Ophthalmol,* 100 (8), e1719-e28.

Bach, M and Hoffmann, M. B. (2006), 'The Origin of the Pattern Electroretinogram', in J. R. Heckenlively and G. B. Arden (eds.), *Principles and Practice of Clinical Electrophysiology of Vision (Second Edition)* (The MIT Press), 185-96.

Barboni, M. T. S., et al. (2024), 'Electroretinographic oscillatory potentials in Leber hereditary optic neuropathy', *Doc Ophthalmol,* 148 (3), 133-43.

Bayer, S., et al. (2025), 'Could a hand-held, visual electrophysiology device theoretically reduce diagnostic waiting times for complex eye conditions in the NHS? A Discrete Event Simulation (DES) modelling study', *BMC Health Serv Res,* 25 (1), 461.

Best, W. and Bohnen, K. (1957), '[Off-effect in electroretinogram of men]', *Albrecht Von Graefes Arch Ophthalmol,* 158 (6), 568-77.

Bhatt, Y., Hunt, D. M., and Carvalho, L. S. (2023), 'The origins of the full-field flash electroretinogram b-wave', *Front Mol Neurosci,* 16, 1153934.

Brigell, M., et al. (2020), 'ISCEV extended protocol for derivation and analysis of the strong flash rod-isolated ERG a-wave', *Doc Ophthalmol,* 140 (1), 5-12.

Brown, K. T. (1968), 'The eclectroretinogram: its components and their origins', *Vision Res,* 8 (6), 633-77.

Brown, K. T. and Wiesel, T. N. (1961), 'Localization of origins of electroretinogram components by intraretinal recording in the intact cat eye', *J Physiol,* 158 (2), 257-80.

Bush, R. A. and Sieving, P. A. (1994), 'A proximal retinal component in the primate photopic ERG a-wave', *Invest Ophthalmol Vis Sci,* 35 (2), 635-45.

Calcagni, A., et al. (2024), 'Electrodiagnostic tests of the visual pathway and applications in neuro-ophthalmology', *Eye (Lond),* 38 (12), 2392-405.

Carter, P., et al. (2021), 'Comparison of the handheld RETeval ERG system with a routine ERG system in healthy adults and in paediatric patients', *Eye (Lond),* 35 (8), 2180-89.

Chiang, T. K., et al. (2022), 'Use of Visual Electrophysiology to Monitor Retinal and Optic Nerve Toxicity', *Biomolecules,* 12 (10).

Cobb, W. A. and Morton, H. B. (1953), 'A new component of the human electroretinogram', *J. Physiol. (Lond),* 123, 36-37.

Cohen, M. X. (2019), 'A better way to define and describe Morlet wavelets for time-frequency analysis', *Neuroimage,* 199, 81-86.

Comander, J., Loewenstein, J., and Sobrin, L. (2011), 'Diagnostic testing and disease monitoring in birdshot chorioretinopathy', *Semin Ophthalmol,* 26 (4-5), 329-36.
Cornish, E. E., et al. (2021), 'The electroretinogram in the genomics era: outer retinal disorders', *Eye (Lond),* 35 (9), 2406-18.
Cruz, R. D., Adachi-Usami, E., and Kakisu, Y. (1990), 'Flash electroretinograms and pattern visually evoked cortical potentials in Behcet's disease', *Jpn J Ophthalmol,* 34 (2), 142-8.
Curcio, C. A., et al. (1990), 'Human photoreceptor topography', *J Comp Neurol,* 292 (4), 497-523.
Dai, J., et al. (2017), 'Contribution of GABAa, GABAc and glycine receptors to rat dark-adapted oscillatory potentials in the time and frequency domain', *Oncotarget,* 8 (44), 77696-709.
Dick, E. and Miller, R. F. (1978), 'Light-evoked potassium activity in mudpuppy retina: its relationship to the b-wave of the electroretinogram', *Brain Res,* 154 (2), 388-94.
--- (1985), 'Extracellular K+ activity changes related to electroretinogram components. I. Amphibian (I-type) retinas', *J Gen Physiol,* 85 (6), 885-909.
Dick, E., Miller, R. F., and Bloomfield, S. (1985), 'Extracellular K+ activity changes related to electroretinogram components. II. Rabbit (E-type) retinas', *J Gen Physiol,* 85 (6), 911-31.
Dmitriev, A. V., Dmitriev, A. A., and Linsenmeier, R. A. (2021), 'K(+)-dependent Muller cell-generated components of the electroretinogram', *Vis Neurosci,* 38, E010.
Dong, C. J., Agey, P., and Hare, W. A. (2004), 'Origins of the electroretinogram oscillatory potentials in the rabbit retina', *Vis Neurosci,* 21 (4), 533-43.
Doty, R. W. and Kimura, D. S. (1963), 'Oscillatory Potentials in the Visual System of Cats and Monkeys', *J Physiol,* 168 (1), 205-18.
Durajczyk, M. and Lubinski, W. (2025), 'Congenital Stationary Night Blindness (CSNB)-Case Reports and Review of Current Knowledge', *J Clin Med,* 14 (4).
Faber, D. S. (1969), 'Analysis of the slow transretinal potentials in response to light', (State University of New York).
Finger, R. P., et al. (2011), 'Prevalence and causes of registered blindness in the largest federal state of Germany', *Br J Ophthalmol,* 95 (8), 1061-7.
Foerster, M. H., van de Grind, W. A., and Grusser, O. J. (1977), 'Frequency transfer properties of three distinct types of cat horizontal cells', *Exp Brain Res,* 29 (3-4), 347-66.
Foerster, M. H., Esser, J., and Laqua, H. (1985), 'Silicone oil and its influence on electrophysiologic findings', *Am J Ophthalmol,* 99 (2), 201-6.
Forshaw, T. R. J., et al. (2022), 'Full-Field Electroretinography Changes Associated with Age-Related Macular Degeneration: A Systematic Review with Meta-Analyses', *Ophthalmologica,* 245 (3), 195-203.
Frishman, L. J. (2006), 'Origins of the Electroretinogram', in J. R. Heckenlively and G. B. Arden (eds.), *Principles and Practice of Clinical Electrophysiology of Vision (Second Edition)* (The MIT Press), 139-83.

Frishman, L. J., et al. (2018), 'ISCEV extended protocol for the photopic negative response (PhNR) of the full-field electroretinogram', *Doc Ophthalmol,* 136 (3), 207-11.
Frishman, L. J., et al. (1996), 'The scotopic electroretinogram of macaque after retinal ganglion cell loss from experimental glaucoma', *Invest Ophthalmol Vis Sci,* 37 (1), 125-41.
Fu, S., et al. (2015), 'Muller Glia Are a Major Cellular Source of Survival Signals for Retinal Neurons in Diabetes', *Diabetes,* 64 (10), 3554-63.
Galuszka, M., Pojda-Wilczek, D., and Karska-Basta, I. (2023), 'Age-Related Macular or Retinal Degeneration?', *Medicina (Kaunas),* 59 (5).
Gouras, P., Eggers, H. M., and MacKay, C. J. (1983), 'Cone dystrophy, nyctalopia, and supernormal rod responses. A new retinal degeneration', *Arch Ophthalmol,* 101 (5), 718-24.
Granit, R. (1933), 'The components of the retinal action potential in mammals and their relation to the discharge in the optic nerve', *J Physiol,* 77 (3), 207-39.
Granit, R. and Munsterhjelm, A. (1937), 'The electrical responses of dark-adapted frogs' eyes to monochromatic stimuli', *J Physiol,* 88 (4), 436-58.
Guite, P. and Lachapelle, P. (1990), 'The effect of 2-amino-4-phosphonobutyric acid on the oscillatory potentials of the electroretinogram', *Doc Ophthalmol,* 75 (2), 125-33.
Gur, M., et al. (1987), 'Changes in the oscillatory potentials of the electroretinogram in glaucoma', *Curr Eye Res,* 6 (3), 457-66.
Gurevich, L. and Slaughter, M. M. (1993), 'Comparison of the waveforms of the ON bipolar neuron and the b-wave of the electroretinogram', *Vision Res,* 33 (17), 2431-5.
Gutierrez, O. and Spiguel, R. D. (1973), 'Oscillatory potentials of the cat retina: effects of adrenergic drugs', *Life Sci,* 13 (7), 991-9.
Hall, Jennifer K. and Volpe, Nicholas J. (2008), 'Autoimmune Retinopathies', in Birgit Lorenz and Francois-Xavier Borruat (eds.), *Pediatric Ophthalmology, Neuro-Ophthalmology, Genetics* (Berlin, Heidelberg: Springer Berlin Heidelberg), 163-83.
Haq, W., et al. (2023), 'Using Micro-Electrode-Array Recordings and Retinal Disease Models to Elucidate Visual Functions: Simultaneous Recording of Local Electroretinograms and Ganglion Cell Action Potentials Reveals the Origin of Retinal Oscillatory Potentials', *Bioengineering (Basel),* 10 (6).
Hayreh, S. S., et al. (1989), 'Electroretinography in central retinal vein occlusion. Correlation of electroretinographic changes with pupillary abnormalities', *Graefes Arch Clin Exp Ophthalmol,* 227 (6), 549-61.
Hempel, F.G. (1972), 'Modification of the Rabbit Electroretinogram by Reserpine', *Ophthalmic Research,* 4 (2), 65-75.
Hirose, T., et al. (1991), 'Retinal function in birdshot retinochoroidopathy', *Acta Ophthalmol (Copenh),* 69 (3), 327-37.
Hoffmann, M. B., et al. (2021), 'ISCEV standard for clinical multifocal electroretinography (mfERG) (2021 update)', *Doc Ophthalmol,* 142 (1), 5-16.
Holder, G. E. (2006), 'The Pattern Electroretinogram', in J. R. Heckenlively and G. B. Arden (eds.), *Principles and Practice of Clinical Electrophysiology of Vision (Second Edition)* (The MIT Press), 341-51.

Hood, D. C. (2000), 'Assessing retinal function with the multifocal technique', *Prog Retin Eye Res,* 19 (5), 607-46.
Hood, D. C., et al. (2002), 'Retinal origins of the primate multifocal ERG: implications for the human response', *Invest Ophthalmol Vis Sci,* 43 (5), 1673-85.
Hope-Ross, M., Mahon, G. J., and Johnston, P. B. (1993), 'Ocular siderosis', *Eye (Lond),* 7 (Pt 3), 419-25.
Huang, Wan-Chun, Liu, Pei-Kang, and Wang, Nan-Kai (2023), 'Electroretinogram (ERG) to Evaluate the Retina in Cases of Retinitis Pigmentosa (RP)', in Stephen H. Tsang and Peter M. J. Quinn (eds.), *Retinitis Pigmentosa* (New York, NY: Springer US), 111-22.
Hug, T. E., Fitzgerald, K. M., and Cibis, G. W. (2000), 'Clinical and electroretinographic findings in fetal alcohol syndrome', *J AAPOS,* 4 (4), 200-4.
Imaizumi, M., et al. (2000), 'Electroretinographic assessment of early changes in ocular siderosis', *Ophthalmologica,* 214 (5), 354-9.
Jacobi, P. C., et al. (1994), 'Neuromodulatory effects of the renin-angiotensin system on the cat electroretinogram', *Invest Ophthalmol Vis Sci,* 35 (3), 973-80.
Jamison, J. A., et al. (2001), 'Characterization of the rod photoresponse isolated from the dark-adapted primate ERG', *Vis Neurosci,* 18 (3), 445-55.
Johnson, M. A., et al. (2019), 'ISCEV extended protocol for the stimulus-response series for the dark-adapted full-field ERG b-wave', *Doc Ophthalmol,* 138 (3), 217-27.
Kang Derwent, J. J. and Linsenmeier, R. A. (2001), 'Intraretinal analysis of the a-wave of the electroretinogram (ERG) in dark-adapted intact cat retina', *Vis Neurosci,* 18 (3), 353-63.
Kannan, N. B., et al. (2016), 'Management of Ocular Siderosis: Visual Outcome and Electroretinographic Changes', *J Ophthalmol,* 2016, 7272465.
Karowski, C. J. and Proenza, L. M. (1977), 'Relationship between Muller cell responses, a local transretinal potential, and potassium flux', *J Neurophysiol,* 40 (2), 244-59.
Keeley, P. W., et al. (2023), 'Is Critical for AII Amacrine Cell Production: Selective Bipolar Cell Dependencies and Diminished ERG', *J Neurosci,* 43 (49), 8367-84.
Keltner, J. L., Thirkill, C. E., and Yip, P. T. (2001), 'Clinical and immunologic characteristics of melanoma-associated retinopathy syndrome: eleven new cases and a review of 51 previously published cases', *J Neuroophthalmol,* 21 (3), 173-87.
Khan, A. O. (2023), 'Full-field electroretinography - when do we need it?', *Saudi J Ophthalmol,* 37 (4), 263-68.
Kim, H. M., Park, K. H., and Woo, S. J. (2020a), 'Correlation of electroretinography components with visual function and prognosis of central retinal artery occlusion', *Sci Rep,* 10 (1), 12146.
--- (2020b), 'Normal to supernormal 30-Hz flicker ERGs predict visual function and prognosis in central retinal artery occlusion', *Doc Ophthalmol,* 141 (3), 279-92.

Knave, B (1969), 'Electroretinography in eyes with retained intraocular metallic foreign bodies : a clinical study', *Acta ophthalmologica : Supplementum 100*, 3-63.

Kojima, M. and Zrenner, E. (1978), 'Off-components in response to brief light flashes in the oscillatory potential of the human electroretinogram', *Albrecht Von Graefes Arch Klin Exp Ophthalmol,* 206 (2), 107-20.

Kolb, H. (2006), 'Functional Organization of the Retina', in J. R. Heckenlively and G. B. Arden (eds.), *Principles and Practice of Clinical Electrophysiology of Vision (Second Edition)* (The MIT Press), 47-64.

Kooijman, A. C., et al. (1991), 'Prolonged electro-retinal response suppression (PERRS) in patients with stationary subnormal visual acuity and photophobia', *Doc Ophthalmol,* 78 (3-4), 245-54.

Korol, S., et al. (1975), 'In vivo effects of glycine on retinal ultrastructure and averaged electroretinogram', *Brain Res,* 97 (2), 235-51.

Lachapelle, P., Little, J. M., and Polomeno, R. C. (1983), 'The photopic electroretinogram in congenital stationary night blindness with myopia', *Invest Ophthalmol Vis Sci,* 24 (4), 442-50.

Lei, B., et al. (2006), 'Study of rod- and cone-driven oscillatory potentials in mice', *Invest Ophthalmol Vis Sci,* 47 (6), 2732-8.

Liao, F., et al. (2023), 'Origin of Retinal Oscillatory Potentials in the Mouse, a Tool to Specifically Locate Retinal Damage', *Int J Mol Sci,* 24 (4).

Liu, C. N., et al. (2014), 'GlyT1 inhibitor reduces oscillatory potentials of the electroretinogram in rats', *Cutan Ocul Toxicol,* 33 (3), 206-11.

Mai, X., et al. (2021), 'Correlation Between Electroretinogram and Visual Prognosis in Metallic Intraocular Foreign Body Injury', *Front Med (Lausanne),* 8, 688305.

Marmor, M. F., et al. (1990), 'Diagnostic clinical findings of a new syndrome with night blindness, maculopathy, and enhanced S cone sensitivity', *Am J Ophthalmol,* 110 (2), 124-34.

Marmor, M. F., et al. (2016), 'Recommendations on Screening for Chloroquine and Hydroxychloroquine Retinopathy (2016 Revision)', *Ophthalmology,* 123 (6), 1386-94.

Massey, S. C., Redburn, D. A., and Crawford, M. L. (1983), 'The effects of 2-amino-4-phosphonobutyric acid (APB) on the ERG and ganglion cell discharge of rabbit retina', *Vision Res,* 23 (12), 1607-13.

McAnany, J. J., Persidina, O. S., and Park, J. C. (2022), 'Clinical electroretinography in diabetic retinopathy: a review', *Surv Ophthalmol,* 67 (3), 712-22.

McCulloch, D. L., et al. (2019), 'ISCEV extended protocol for the stimulus-response series for light-adapted full-field ERG', *Doc Ophthalmol,* 138 (3), 205-15.

McKellar, M. J., Hidajat, R. R., and Elder, M. J. (1997), 'Acute ocular methanol toxicity: clinical and electrophysiological features', *Aust N Z J Ophthalmol,* 25 (3), 225-30.

Meigen, T. and Bach, M. (2006), 'Electrophysiology in the Diagnosis of Glaucoma', in Franz Grehn and Robert Stamper (eds.), *Glaucoma* (Berlin, Heidelberg: Springer Berlin Heidelberg), 73-90.

Michaelides, M., et al. (2005), 'A detailed phenotypic study of "cone dystrophy with supernormal rod ERG"', *Br J Ophthalmol,* 89 (3), 332-9.
Midena, E., et al. (2021), 'Early Microvascular and Oscillatory Potentials Changes in Human Diabetic Retina: Amacrine Cells and the Intraretinal Neurovascular Crosstalk', *J Clin Med,* 10 (18).
Miller, R. F. and Dowling, J. E. (1970), 'Intracellular responses of the Muller (glial) cells of mudpuppy retina: their relation to b-wave of the electroretinogram', *J Neurophysiol,* 33 (3), 323-41.
Miyake, Y. (2006), 'Complete and Incomplete Types of CSNB', *Electrodiagnosis of Retinal Diseases* (Tokyo: Springer Tokyo), 90-113.
Moller, A. and Eysteinsson, T. (2003), 'Modulation of the components of the rat dark-adapted electroretinogram by the three subtypes of GABA receptors', *Vis Neurosci,* 20 (5), 535-42.
Morita, Y. (1971), '[Effects of temperature and sodium aspartate on the ERG of the albino rabbit retina]', *Nippon Ganka Gakkai Zasshi,* 75 (3), 1071-5.
Moschos, M. M., Gouliopoulos, N. S., and Kalogeropoulos, C. (2014), 'Electrophysiological examination in uveitis: a review of the literature', *Clin Ophthalmol,* 8, 199-214.
Naarendorp, F. and Williams, G. E. (1999), 'The d-wave of the rod electroretinogram of rat originates in the cone pathway', *Vis Neurosci,* 16 (1), 91-105.
Neveu, M. M., et al. (2025), 'Electrodiagnostic Tests as Potential Efficacy Endpoints in Clinical Trials of Novel Pharmacological Therapies for Acquired Retinal Disorders', *Ophthalmic Res,* 68 (1), 169-86.
Newman, E. A. (1993), 'Inward-rectifying potassium channels in retinal glial (Muller) cells', *J Neurosci,* 13 (8), 3333-45.
Newman, E. A. and Odette, L. L. (1984), 'Model of electroretinogram b-wave generation: a test of the K+ hypothesis', *J Neurophysiol,* 51 (1), 164-82.
O'Neill, E. K. and Smith, R. (2021), 'Visual electrophysiology in the assessment of toxicity and deficiency states affecting the visual system', *Eye (Lond),* 35 (9), 2344-53.
Ogden, T. E. (1973), 'The oscillatory waves of the primate electroretinogram', *Vision Res,* 13 (6), 1059-74.
Ogden, T. E. and Wylie, R. M. (1971), 'Avian retina. I. Microelectrode depth and marking studies of local ERG', *J Neurophysiol,* 34 (3), 357-66.
Pasmanter, N. and Petersen-Jones, S. M. (2022), 'Characterization of scotopic and mesopic rod signaling pathways in dogs using the On-Off electroretinogram', *BMC Vet Res,* 18 (1), 422.
Peachey, N. S., Alexander, K. R., and Fishman, G. A. (1987), 'Rod and cone system contributions to oscillatory potentials: an explanation for the conditioning flash effect', *Vision Res,* 27 (6), 859-66.
Penn, R. D. and Hagins, W. A. (1969), 'Signal transmission along retinal rods and the origin of the electroretinographic a-wave', *Nature,* 223 (5202), 201-4.
Perlman, I. (1995), 'The Electroretinogram: ERG', in H. Kolb, et al. (eds.), *Webvision: The Organization of the Retina and Visual System* (Salt Lake City (UT): University of Utah Health Sciences Center Copyright: © 2025 Webvision .).

Perlman, I., et al. (2020), 'ISCEV extended protocol for the S-cone ERG', *Doc Ophthalmol,* 140 (2), 95-101.
Pohlmann, D., Winterhalter, S., and Pleyer, U. (2019), '[White dot syndromes : Principles, diagnostics, and treatment]', *Ophthalmologe,* 116 (12), 1235-56.
Preiser, D., et al. (2013), 'Photopic negative response versus pattern electroretinogram in early glaucoma', *Invest Ophthalmol Vis Sci,* 54 (2), 1182-91.
Qu, Y., et al. (2024), 'Oscillatory potential findings in patients with acute ischaemic central retinal vein occlusion', *BMJ Open Ophthalmol,* 9 (1).
Righetti, G., et al. (2025), 'Investigating the OFF-pathway contribution to oscillatory potentials in the human ERG in ’Abstracts of the 62nd annual symposium of the international society for clinical electrophysiology of vision (ISCEV 2025), Utrecht, the Netherlands’', *Documenta Ophthalmologica,* 150 (1), 44.
Righetti, G., et al. (2021), 'Oscillatory Potentials in Achromatopsia as a Tool for Understanding Cone Retinal Functions', *Int J Mol Sci,* 22 (23).
Robson, A. G., et al. (2018), 'ISCEV guide to visual electrodiagnostic procedures', *Doc Ophthalmol,* 136 (1), 1-26.
Robson, A. G., et al. (2022), 'ISCEV Standard for full-field clinical electroretinography (2022 update)', *Doc Ophthalmol,* 144 (3), 165-77.
Robson, J. G. and Frishman, L. J. (1998), 'Dissecting the dark-adapted electroretinogram', *Doc Ophthalmol,* 95 (3-4), 187-215.
Robson, J. G., et al. (2003), 'Rod and cone contributions to the a-wave of the electroretinogram of the macaque', *J Physiol,* 547 (Pt 2), 509-30.
Rousseau, S. and Lachapelle, P. (1999), 'The electroretinogram recorded at the onset of dark-adaptation: understanding the origin of the scotopic oscillatory potentials', *Doc Ophthalmol,* 99 (2), 135-50.
Sabbaghi, H., et al. (2021), 'New criteria for evaluation of electroretinogram in patients with retinitis pigmentosa', *Doc Ophthalmol,* 143 (3), 271-81.
Sakata, V. M., et al. (2019), 'Full-field electroretinogram behavior in Vogt-Koyanagi-Harada disease: a 24-month longitudinal study in patients from acute onset evaluated with multimodal analysis', *Graefes Arch Clin Exp Ophthalmol,* 257 (10), 2285-95.
Schechner, R., et al. (1990), 'A long term follow up of ocular siderosis: quantitative assessment of the electroretinogram', *Doc Ophthalmol,* 76 (3), 231-40.
Sergott, R. C. and Westall, C. A. (2011), 'Primer on visual field testing, electroretinography, and other visual assessments for patients treated with vigabatrin', *Acta Neurol Scand Suppl,* (192), 48-56.
Sieving, P. A., Murayama, K., and Naarendorp, F. (1994), 'Push-pull model of the primate photopic electroretinogram: a role for hyperpolarizing neurons in shaping the b-wave', *Vis Neurosci,* 11 (3), 519-32.
Sillman, A. J., Ito, H., and Tomita, T. (1969), 'Studies on the mass receptor potential of the isolated frog retina. I. General properties of the response', *Vision Res,* 9 (12), 1435-42.
Skaat, A., et al. (2011), 'Increased electroretinogram a-wave amplitude after intravitreal bevacizumab injection for neovascular age-related macular degeneration', *Acta Ophthalmol,* 89 (3), e269-73.

Steinberg, R. H. (1966), 'Oscillatory activity in the optic tract of cat and light adaptation', *J Neurophysiol,* 29 (2), 139-56.
Stockton, R. A. and Slaughter, M. M. (1989), 'B-wave of the electroretinogram. A reflection of ON bipolar cell activity', *J Gen Physiol,* 93 (1), 101-22.
Sustar, M., et al. (2018), 'ISCEV extended protocol for the photopic On-Off ERG', *Doc Ophthalmol,* 136 (3), 199-206.
Thompson, D. A., et al. (2018), 'ISCEV extended protocol for the dark-adapted red flash ERG', *Doc Ophthalmol,* 136 (3), 191-97.
Thompson, D. A., et al. (2024), 'ISCEV standard for clinical pattern electroretinography (2024 update)', *Doc Ophthalmol,* 148 (2), 75-85.
Tremblay, F. and Lam, S. R. (1993), 'Distinct electroretinographic oscillatory potential generators as revealed by field distribution', *Doc Ophthalmol,* 84 (3), 279-89.
Tsang, Stephen H. and Sharma, Tarun (2018), 'Electroretinography', in Stephen H. Tsang and Tarun Sharma (eds.), *Atlas of Inherited Retinal Diseases* (Cham: Springer International Publishing), 17-20.
Ueno, S., et al. (2006), 'Contribution of retinal neurons to d-wave of primate photopic electroretinograms', *Vision Res,* 46 (5), 658-64.
Vaegan and Millar, T. J. (1994), 'Effect of kainic acid and NMDA on the pattern electroretinogram, the scotopic threshold response, the oscillatory potentials and the electroretinogram in the urethane anaesthetized cat', *Vision Res,* 34 (9), 1111-25.
Vaegan, et al. (1995), 'Flash and pattern electroretinogram changes with optic atrophy and glaucoma', *Exp Eye Res,* 60 (6), 697-706.
Vincent, A., Robson, A. G., and Holder, G. E. (2013), 'Pathognomonic (diagnostic) ERGs. A review and update', *Retina,* 33 (1), 5-12.
Wachtmeister, L. (1980), 'Further studies of the chemical sensitivity of the oscillatory potentials of the electroretinogram (ERG) I. GABA- and glycine antagonists', *Acta Ophthalmol (Copenh),* 58 (5), 712-25.
--- (1981a), 'Further studies of the chemical sensitivity of the oscillatory potentials of the electroretinogram (ERG). II. Glutamate-aspartate-and dopamine antagonists', *Acta Ophthalmol (Copenh),* 59 (2), 247-58.
--- (1981b), 'Further studies of the chemical sensitivity of the oscillatory potentials of the electroretinogram (ERG). III. Some omega amino acids and ethanol', *Acta Ophthalmol (Copenh),* 59 (4), 609-19.
--- (1983), 'The action of peptides on the mudpuppy electroretinogram (ERG)', *Exp Eye Res,* 37 (5), 429-37.
--- (1998), 'Oscillatory potentials in the retina: what do they reveal', *Prog Retin Eye Res,* 17 (4), 485-521.
Wachtmeister, L. and Dowling, J. E. (1978), 'The oscillatory potentials of the mudpuppy retina', *Invest Ophthalmol Vis Sci,* 17 (12), 1176-88.
Wachtmeister, L. and el Azazi, M. (1985), 'Oscillatory potentials of the electroretinogram in patients with unilateral optic atrophy', *Ophthalmologica,* 191 (1), 39-50.
Wanger, P. and Persson, H. E. (1983), 'Pattern-reversal electroretinograms in unilateral glaucoma', *Invest Ophthalmol Vis Sci,* 24 (6), 749-53.
Wässle, H., et al. (2009), 'Glycinergic transmission in the Mammalian retina', *Front Mol Neurosci,* 2, 6.

Wen, R. and Oakley, B., 2nd (1990), 'K(+)-evoked Muller cell depolarization generates b-wave of electroretinogram in toad retina', *Proc Natl Acad Sci U S A,* 87 (6), 2117-21.

Williamson, T. H., Keating, D., and Bradnam, M. (1997), 'Electroretinography of central retinal vein occlusion under scotopic and photopic conditions: what to measure?', *Acta Ophthalmol Scand,* 75 (1), 48-53.

Xie, X., et al. (2022), 'Comprehensive visual electrophysiological measurements discover crucial changes caused by alcohol addiction in humans: Clinical values in early prevention of alcoholic vision decline', *Front Neural Circuits,* 16, 912883.

Xu, X. and Karwoski, C. J. (1994), 'Current source density analysis of retinal field potentials. II. Pharmacological analysis of the b-wave and M-wave', *J Neurophysiol,* 72 (1), 96-105.

Xu, X. and Karwoski, C. (1995), 'Current source density analysis of the electroretinographic d wave of frog retina', *J Neurophysiol,* 73 (6), 2459-69.

Yanagida, T., et al. (1986), 'Microelectrode depth study of electroretinographic b- and d-waves in frog retina', *Jpn J Ophthalmol,* 30 (3), 298-305.

Yang, Y., et al. (2019), 'Tmem30a deficiency leads to retinal rod bipolar cell degeneration', *J Neurochem,* 148 (3), 400-12.

Yap, G. H., et al. (2015), 'Clinical value of electrophysiology in determining the diagnosis of visual dysfunction in neuro-ophthalmology patients', *Doc Ophthalmol,* 131 (3), 189-96.

Yu, M. and Kurup, S. K. (2024), 'Application of Ophthalmic Electrophysiology in Inflammatory Disorders of Retina and Optic Nerve', *J Clin Med,* 13 (13).

Yu, M., et al. (2025), 'The Role of Visual Electrophysiology in Systemic Hereditary Syndromes', *Int J Mol Sci,* 26 (3).

Zeitz, C., et al. (2018), '[Overview of Congenital Stationary Night Blindness with Predominantly Normal Fundus Appearance]', *Klin Monbl Augenheilkd,* 235 (3), 281-89.

Zhou, W., et al. (2007), 'Oscillatory potentials of the slow-sequence multifocal ERG in primates extracted using the Matching Pursuit method', *Vision Res,* 47 (15), 2021-36.

8 Erklärung zum Eigenanteil

Die Arbeit wurde in der Universitäts-Augenklinik Tübingen unter Betreuung von PD Dr. rer. nat. Krunoslav Stingl und Giulia Righetti durchgeführt.

Die Konzeption der Studie und des Messprotokolls erfolgte in Zusammenarbeit mit PD Dr. rer. nat. Krunoslav Stingl und Giulia Righetti.

Die Versuche wurden nach Einarbeitung durch Giulia Righetti von mir eigenständig durchgeführt.

Die statistische und graphische Auswertung der Studienergebnisse wurde von mir unter Hilfestellung von Giulia Righetti durchgeführt.

Die Abbildungen 3-11 wurden von mir unter Hilfestellung von Giulia Righetti erstellt. Abbildungen 1 und 2 wurden aus den jeweils angegebenen Publikationen entnommen und entsprechend gekennzeichnet.

Aus der Dissertation ging der Abstract „Investigating the OFF-pathway contribution to oscillatory potentials in the human ERG“ für das ISCEV Symposium hervor. Die zugrundeliegenden Versuche wurden nach Einarbeitung durch Giulia Righetti von mir durchgeführt. Die Konzeption und Niederschrift erfolgte durch Giulia Righetti in Zusammenarbeit mit den Co-Autoren und mir.

Die Dissertationsschrift wurde selbst durch mich erstellt.

Ich versichere, das Manuskript selbständig verfasst zu haben und keine weiteren als die von mir angegebenen Quellen verwendet zu haben.

Tübingen, den 23.01.2026

Johannes Karl Andreas David Passauer

9 Veröffentlichungen

Teile der vorliegenden Dissertationsschrift wurden bereits in der unten genannten Publikation veröffentlicht. In der vorliegenden Arbeit sind diese mit der Zitierung (Righetti et al. 2025) gekennzeichnet.

Righetti, G., et al. (2025), 'Investigating the OFF-pathway contribution to oscillatory potentials in the human ERG in ’Abstracts of the 62nd annual symposium of the international society for clinical electrophysiology of vision (ISCEV 2025), Utrecht, the Netherlands'', *Documenta Ophthalmologica,* 150 (1), 44.

10 Danksagung

Für die exzellente Betreuung möchte ich mich bei Privatdozent Dr. rer. nat. K. Stingl, Prof. Dr. med. Katarina Stingl und ganz besonders bei Giulia Righetti bedanken.

Ein großes Dankeschön gilt allen Probandinnen und Probanden für ihre Zeit, Geduld und Bereitschaft.

Von Herzen möchte ich mich bei Andrea, Andreas, Helga, Gerhard, Samuel, Stefanie und Natalie für eure unermesslich große Unterstützung bedanken.